

Evidence for Multi-Rifting in the Variscan-Alpine Cycle Transition: Insights from the European western Southern Alps

Emanuele Scaramuzzo¹, Franz A. Livio¹, Maria Giuditta Fellin², Colin Maden²

¹Department of Science and High Technology, University of Insubria, via Valleggio 11, 22100 Como, Italy

²Department of Earth and Planetary Sciences, ETH Zürich, Sonneggstrasse 5, 8092 Zurich, Switzerland.

Correspondence to: M.G. Fellin (fellin@eaps.ethz.ch)

Abstract. We investigate the transition between the Paleozoic Variscan cycle and the Meso-Cenozoic Alpine supercontinent cycle, both of which have played a pivotal role in shaping the central European-Mediterranean plate architecture. Two main scenarios have been proposed so far for this transition: i) a single, long-lasting, Permo-Triassic rifting event, culminating in the opening of the Alpine Tethys, or ii) multiple, distinct rifting events, predating the onset of the Alpine cycle. Our study focuses on the European western Southern Alps (Varese Area, N Italy), where we document the tectonic events from the early Permian to the Middle Triassic. Through a combined tectono-stratigraphic and thermochronological analysis, we identify an initial early Permian rifting stage, linked to magmatic activity, followed by early-middle Permian transcurrent tectonics. This phase is truncated by a middle Permian regional-scale erosional event that marks the cessation of this tectonic phase. Subsequently, during the Middle Triassic, a second phase initiated, which we interpret as the onset of the Alpine Tethys opening. This phase likely corresponds to an early stretching stage that predates the well-documented Late Triassic crustal-thinning phase. Based on our findings, we propose that the Middle Triassic stretching phase represents the first stage of the Alpine Tethys rifting, thereby challenging the hypothesis of a continuous Permo-Triassic long-lasting extension.

1 Introduction

The Paleozoic Variscan cycle and the successive Mesozoic-Cenozoic Alpine supercontinent cycle (sensu Wilson, 1968; Wilson et al., 2019, and references therein) have shaped the structural framework of the central European-Mediterranean plate (e.g., Stampfli and Kozur 2006; Ballèvre et al., 2020; Elter et al., 2020; Molli et al., 2020). Due to the large hiatus in the geological record spanning from the latest Paleozoic to the earliest Mesozoic, the transition between the two cycles is open to different interpretations. As a remnant of the Variscan chain (Figure 1a), the European Southern Alps stand as an ideal study area to unravel the geodynamic processes governing the transition between the two cycles. In this region, three main events took place during this transition.

Firstly, the deposition of an upper Carboniferous siliciclastic cover on the Variscan metamorphic basement was followed by early Permian crustal thinning and cal-alkaline magmatism throughout the former peri-Variscan chain (e.g., Stampfli, 1996, 2000; Ziegler and Stampfli, 2001; Stampfli and Kozur, 2006; Cassinis et al., 2012; Cassinis et al., 2018; Ballèvre et al., 2020;

Deleted: tectonic

Deleted: phase

Deleted: end of the Variscan cycle

Molli et al., 2020). Then, a non-depositional, erosive phase cut through this succession all around the Mediterranean area during the early-middle Permian (e.g., Cassinis et al., 2012; Gretter et al., 2013; Cassinis et al., 2018 and references therein).

35 The resulting erosive surface was later covered by discontinuous, upper-middle Permian to Lower Triassic continental to shallow water marine sediments followed by discontinuous platforms and intra-platform basins successions (e.g., Bernoulli, 2007; Gaetani, 2010 and references therein). Finally, crustal thinning started in the Late Triassic (e.g., Bertotti et al., 1993). Two main scenarios have been postulated so far to explain how the transition between the Variscan and the Alpine cycles occurred: in the first scenario, the succession of events described above relate to a long-lasting, single-rifting event between

40 the demise of the Variscan cycle in the late Carboniferous and the onset of the Alpine one in the Late Triassic (e.g., Winterer and Bosellini, 1981; Siletto et al., 1993; Zanon and Spalla, 2018; Roda et al., 2019). In the alternative scenario, successive and distinct rifting events (hereafter referred to as multi-rifting) intervened between the two cycles (e.g., [Ziegler and Stampfli, 2001](#); Stampfli et al., 2002; Stampfli and Kozur, 2006 and reference therein) and the break between the two cycles occurred at the end of the transition, in the Triassic. According to the single rifting model, the early Permian tectonic phase represents the

45 onset of a single, long-lasting rifting event, under the same plate kinematic framework, culminating with the opening of the Alpine Tethys (e.g., Winterer and Bosellini, 1981; Siletto et al., 1993; Zanon and Spalla, 2018; Roda et al., 2019). Conversely, according to the multi-rifting model, the Late Triassic opening of the Alpine Tethys was preceded by a series of aborted rifting events, taking place under diverse plate kinematic directions (e.g., Ziegler and Stampfli, 2001; Stampfli and Kozur, 2006, and references therein). Several models are concordant with the multi-rifting hypothesis, but each one proposes different

50 mechanisms to explain the succession of distinct rifting events from the early Permian to the Middle Triassic. For instance, Muttoni et al. (2003; 2009) and Schaltegger and Brack (2007) concluded that multi-rifting reflects wrench tectonics related to the reconfiguration of Pangea from an Irving-type (Pangea B) to a Wegener-type (Pangea A). Alternatively, Malavieille et al. (1990) suggested that extension in the early Permian was caused by the orogenic collapse of the Variscan chain. Finally, the early Permian extension could reflect back-arc thinning triggered by the subduction of the Paleotethys ocean beneath the

55 southeastern margin of the Pangea continent (Visonà, 1982; Lorenz and Nicholls, 1984; Stille and Buletti, 1987; Di Battistini et al., 1988; Finger and Steyrer, 1990, 1991; Bonin et al., 1993; Doglioni, 1995; Stampfli and Kozur, 2006). A combined tectono-stratigraphic and low-temperature thermochronological approach on a sector of the former Variscan chain accreted within the western sector of the Southalpine chain here provides novel constraints on the Variscan-Alpine cycles transition. The pristine geological and thermochronological record of the study area shows that the Variscan-Alpine orogenic

60 cycle changeover is marked by a [main aborted rifting phase](#), separated by a transcurrent phase, thus supporting the multi-rifting interpretation.

Deleted: Ziegler and Stampfli, 2001

Deleted: ;

Deleted: main aborted rifting phases

65 2 Geological background

2.1 Regional tectonic framework

The Southern Alps stand as a remnant of the Variscan chain (Figure 1a) that underwent rifting during the Mesozoic, ultimately transforming into the distant passive margin of the northern sector of the Africa Plate, e.g., Adria (e.g., Zingg et al., 1990; Bertotti et al., 1993; Handy et al., 1999; [Ferrando et al., 2004](#); Bernoulli, 2007; Schaltegger and Brack, 2007). This belt is composed of Adria derived units stacked along alpine south-verging thrusts, which accommodated reduced shortening in the west (Rosenberg and Kissling 2014), locally reactivating inherited structures a(Figure 1b, c; e.g., Scaramuzzo et al., 2022). The fragments of the Variscan chain exposed in the Southern Alps are made up of an assemblage of several tectono-metamorphic units (e.g., Diella et al., 1992; [Siletto et al., 1993](#); Boriani and Villa, 1997; Di Paola et al., 2001; [Boriani et al., 2003](#); Spalla et al., 2006). In the study area, these units consist of amphibolitic facies, para- and ortho-gneisses, and schists (Serie dei Laghi Unit; e.g., Boriani et al., 1990; Handy et al., 1999; Figure 3). These experienced peak metamorphism in the early Carboniferous (340-320 Ma) and cooled to moderate temperatures in the late Carboniferous (ca. 305 Ma), when they reached middle crustal depths, as documented by Rb-Sr age on white mica and biotite (Figure 1d; Schaltegger and Brack, 2007, and references therein). The top of the Variscan basement is marked by a regional erosional surface, the Hercynian Unconformity (Handy et al., 1999). This is overlain locally by Middle Pennsylvanian (ca. 310 Ma) continental conglomerates (i.e., Manno Conglomerate and Mesenzana Fm., Figure 1d; Jongmans 1960; Casati, 1978; Cassinis et al., 2012). During the early Permian (i.e., between 285 and 275 Ma), mafic to acid plutonic rocks with mantle melt involvement intruded the peri-Variscan metamorphic rocks at lower to upper crustal depths (Figure 1d; Barth et al., 1994; Schaltegger and Brack, 2007; Cassinis et al., 2012; [Berra et al., 2015](#); Karakas et al., 2019). This magmatic activity was accompanied by the deposition within caldera complexes of thick successions of volcanic products with calc-alkaline affinity together with clastic continental sediments (Collio, Orobic and Tregiovo basins and Athesian and Sesia Valley caldera; Figure 1d; Bakos et al., 1990; Schaltegger and Brack 2007; Marocchi et al., 2008; Quick et al., 2009; Berra et al., 2015; Berra et al., 2016). In the study area, the lower Permian intrusive rocks consist of aplitic microgranites, granites, and quartz-bearing, NE-SW striking, micro-porphyric dikes, which altogether form a subvolcanic complex (i.e., Ganna Granitic Stock; Baggio and De Marco, 1960; Govi, 1960; Stille and Buletti, 1987; Bakos et al., 1990; Schaltegger and Brack 2007). The emplacement of the Ganna Granitic complex occurred at 281.34 ± 0.48 Ma (Schaltegger and Brack, 2007), near the surface, at pressures most likely in the range of 0.5 – 0.75 kbar and certainly less than 2 kbar (Bakos et al., 1990) implying a maximum thickness of the units overlying the intrusive complex of 2-5 km. Tuffs, ignimbrites and andesitic to dacitic lavas with thin intercalations of clastic rocks of lower Permian age are extensively exposed in the study area (Baggio and De Marco, 1960; Govi, 1960; Stille and Buletti, 1987; Bakos et al., 1990; Schaltegger and Brack 2007).

Deleted: Boriani et al., 2003;

Deleted: Berra et al., 2015;

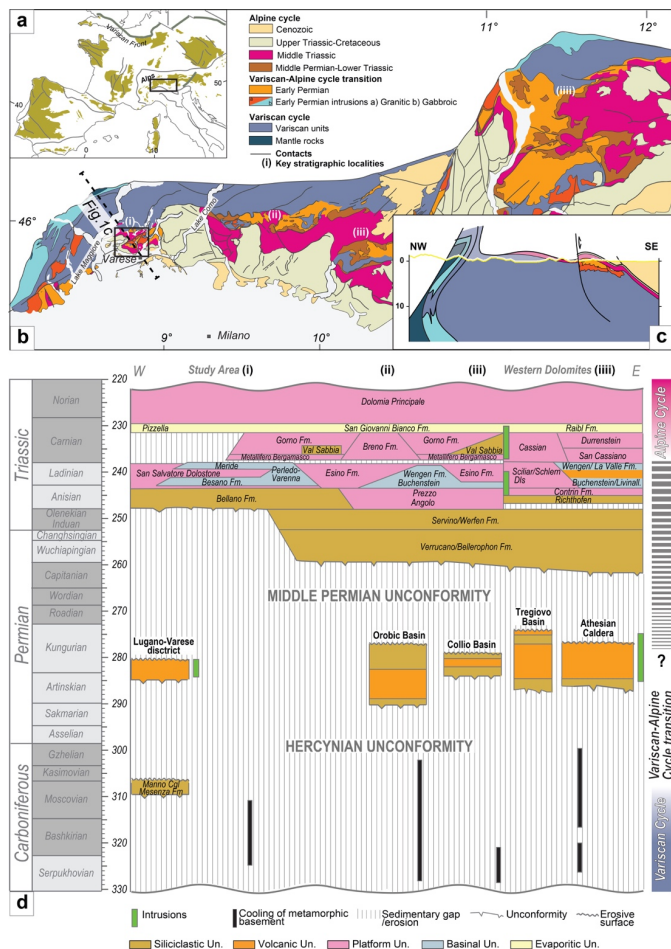


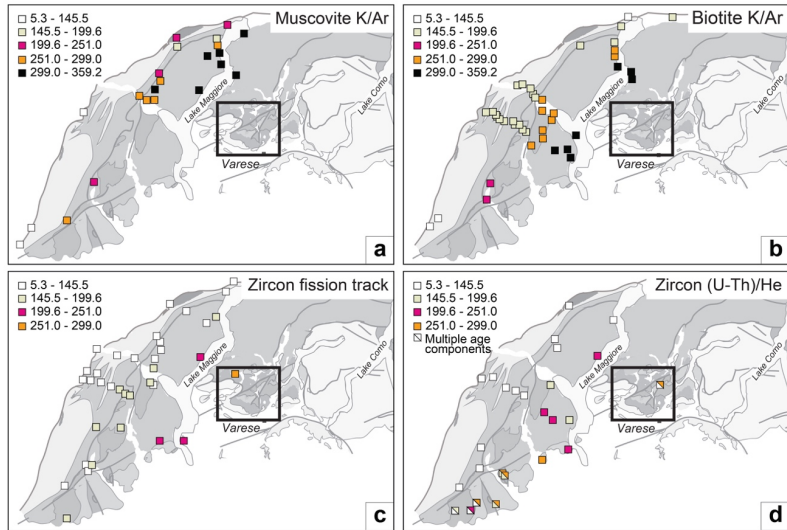
Figure 1: Regional geological setting and stratigraphy: a) distribution of the Palaeozoic peri-Variscan terrain in the Mediterranean area (modified after von Raumer et al., 2002); b) simplified geological map of the Southern Alps modified after Bigi et al., 1990; c) crustal-scale cross-section along the western sector of the Southern Alps (redrawn after Scaramuzzo et al., 2022); d) chronostratigraphic scheme of Carboniferous-Jurassic succession of the Southern Alps with the sequence subdivision adopted in this paper for the study area (redrawn after Schalteger and Brack, 2007; Berra et al., 2009; Cassinis et al., 2012; Gretter et al., 2013; Beltrando et al., 2015; Cassinis et al., 2018).

Across the Southern Alps, a middle Permian erosive surface (the “middle Permian Unconformity”, hereafter; Figure 1d) lies over the top of the exhumed composite metamorphic basement and the lower Permian succession, marking a depositional hiatus of ca. 15 to 20 million years (Figure 1d; e.g., Bernoulli, 2007; Schaltegger and Brack 2007; Gaetani, 2010; Cassinis et al., 2012; Gretter et al., 2013; Cassinis et al., 2018). At middle crustal levels, pervasive extensional deformation is recorded during the middle-late Permian by the metamorphic basement north of the Lake Como (Real et al., 2023). The middle Permian Unconformity is overlain by a diachronous sedimentary wedge consisting of continental siliciclastic deposits and minor coastal marine sediments, which spans from the uppermost middle Permian to the Lower-Middle Triassic (Figure 1d; i.e., Verrucano Fm. and Servino Fm.; e.g., Bernoulli, 2007; Gaetani, 2010; Cassinis et al., 2012; Cassinis et al., 2018). During the Anisian stage, mixed carbonate/fine siliciclastic deposits were deposited over an extensive area (e.g., Gaetani et al., 1988; Brack and Rieber, 1993; Bernoulli, 2007; Gaetani, 2010). In the study area, the Anisian siliciclastic deposits consist of microconglomerates with centimetric rounded quartz clasts dispersed in a red matrix, and of thin-bedded siltstones and fine sandstones with plane-parallel or cross laminations (i.e., Bellano Fm; Figure 1d; Stockar et al., 2013). At the middle-upper Anisian boundary, siliciclastic deposition ended throughout the Southern Alps and substantial carbonate platform grew in proximal areas and alternated with intra-platform basins, which hosted anoxic sediments at once with volcanic activity (Figure 1d; e.g., Gaetani et al., 1988; Brack and Rieber, 1993; Bernoulli, 2007; Gaetani, 2010; Stork et al., 2019; De Min et al., 2020). During this stage, the local formations consist of dolomitic limestones that were deposited in reef and shallow-sea environments (Dolomia di San Salvatore) and that are laterally heteropic with intra-platform limestones and anoxic shales (Meride Limestones and Besano Shales; Figures 1d; Bernoulli 1964; Zorn, 1971; Furrer, 1995; Bernoulli, 2007; Stockar, 2010; Stockar et al., 2013; Renesto and Stockar, 2018). The end of the Carnian is marked across the Southern Alps by the deposition of terrigenous, evaporitic, and lesser carbonate sediments associated with sea-level fall together with the input of siliciclastic and volcanic detritus (Figure 1d; i.e., Pizzella Marls, San Giovanni Bianco Fm., Raibl Fm.; e.g., Bernoulli et al, 2007; Gaetani et al., 2010). The late Anisian to early Carnian development and emersion of carbonate platform was simultaneous with a thermal event recorded by the basement rocks north of the Lake Como, which underwent static recrystallization (Real et al., 2023). During the latest Carnian, the subsidence rate gradually decreased, and the volcanic activity ceased (e.g., Bernoulli, 2007; Gaetani, 2010). Subsidence resumed in the Norian and increased rapidly as crustal thinning progressed (e.g., Bertotti et al., 1993; Gaetani et al., 2010).

2.2 Thermochronological record

The thermochronologic record of the units accreted within the Southalpine chain (Figure 2) spans from the Carboniferous Period to the Miocene Epoch. Most commonly, the lowest temperature (low-T) thermochronometric data, including fission-track and (U-Th)/He ages on apatite and zircon, record the thermal overprint related to the Mesozoic and Cenozoic events of the Alpine cycle (Giger, 1991; Martin et al., 1998; Bertotti et al., 1999; Zattin et al., 2006; Siegesmund et al., 2008; Zanchetta et al., 2011; 2015; Berger et al., 2012; Pomella et al., 2012; Reverman et al., 2012; Wolff et al., 2012; Bertrando et al., 2015; Heberer et al, 2016). Higher temperature (high-T) thermochronometric systems, like Rb/Sr, K/Ar, and Ar/Ar, record also older

140 events that locally date back to the end of the Variscan cycle during the Carboniferous (Figure 2a, b; McDowell and Schmid, 1968; McDowell, 1970; Bertotti et al., 1999; Siegesmund et al., 2008; Zanchetta et al., 2011; Wolff et al., 2012). In the central sector of the Southern Alps area, near Lake Como, Jurassic to Early Cretaceous zircon fission-track ages (Figure 2c) indicate continued cooling from rifting until the onset of Alpine convergence, whereas Late Triassic to Jurassic high-T thermochronometric ages (Rb/Sr and Ar/Ar) document altered thermal conditions before and at the onset of rifting (Bertotti et al., 1999). In the western sector of the Southern Alps, west of Lake Maggiore, apatite fission-track ages are all Eocene and younger, whereas fission-track and (U-Th)/He ages on zircon are Triassic to Miocene, and high-T thermochronometric ages (muscovite and biotite K/Ar; Figure 2a, b) are Carboniferous to Jurassic (McDowell and Schmid, 1968; McDowell, 1970; Hurford, 1986; Siegesmund et al., 2008; Wolff et al. 2012). In the westernmost sector of the Southern Alps, bedrock and detrital zircon (U-Th)/He ages (Figure 2d) record a protracted thermal history that starts in the Late Triassic in relation to crustal thinning and continues until the Cretaceous resulting in wide and complex age distributions in both bedrock and detrital samples (Beltrando et al., 2015).



150 **Figure 2:** a) Muscovite K/Ar ages compiled from McDowell, 1970; Hunziker, 1974; Zwingmann, 2004; Wolff et al., 2012; b) Biotite K/Ar ages compiled from Jager and Faul, 1960; Carraro and Ferrara, 1968; McDowell, 1968; McDowell, 1970; Hunziker, 1974; Hurford, 1986; Siegesmund et al., 2008; Wolff et al., 2012; c) Zircon fission track ages compiled from Hurford, 1986; Bertotti et al., 1999; Siegesmund et al., 2008; Wolff et al., 2012; d) Zircon (U-Th)/He ages compiled from Wolff et al., 2012; Beltrando et al., 2015. Sample with multiple age components are from detrital rocks and partially reset basement rocks (Beltrando et al., 2015).

155

160 Ultimately, among the previous low-T thermochronometric data of the Southern Alps, the few Permian ages so far recorded are from two groups of samples consisting mostly of volcanic and detrital rocks and including one basement sample. One group of samples is located south-west of Lake Maggiore, where Permian volcanics and Jurassic sandstones give zircon (U-Th)/He ages that scatter over a very long temporal interval from the latest Carboniferous to the Late Cretaceous (Beltrando et al., 2015), indicating a low-temperature, protracted thermal history that causes variable age-resetting conditions. The second group of samples is in the Varese area and includes a 256 Ma-old zircon fission-track age in a schist (Giger, 1991) and a zircon (U-Th)/He age cluster between 300 Ma and 250 Ma combined with a Late Cretaceous age cluster in a Permian volcanoclastic rock (Beltrando et al., 2015). Thus, also this second group of samples has a complex thermochronologic record straddling age-resetting conditions.

165 **3 Methods**

3.1 Tectono-stratigraphy and thickness analysis

In this work, we focused on the tectonostratigraphic evolution from the Carboniferous to the Late Triassic, encompassing the end of the Variscan cycle and the onset of the Alpine cycle. This reconstruction builds on prior studies of the tectono-stratigraphy of the Southern Alps (e.g., Bernoulli, 1964; Bertotti et al., 1993; Gaetani et al., 1998; Berra et al., 2009; Cassini et al., 2012) and on the results from our geological mapping that we used to measure stratigraphic successions, to identify crosscut relationships among structures, and to map key horizons and unconformities. Geologic structures were extrapolated at depth by means of a series of geological cross-sections (see Section 4.1 for the tectono-stratigraphy).

A quantitative approach based on a thickness analysis was adopted for the reconstruction of the basin morphology during the inception of the rifting Alpine stage. Specifically, we focussed on the Middle Triassic and on the development of a fault-bounded basin within the Varese area at that time, as we identified this geologic event as essential to understand the onset of the Alpine cycle. We built 25 geological cross-sections (locations in Figure 4c) that informed a 3D geologic model, developed using the MOVE software (courtesy of Petroleum Experts Ltd). The model is composed of mesh surfaces representing the top horizons of stratigraphic units and fault surfaces. These mesh surfaces are available as 3D pdf file in supplementary material (S1). The horizons from the geological cross-sections were interpolated within each fault-bounded structural block and across sections, by means of a spline interpolation method, to minimize curvature away from fault zones. Each structural block was then progressively restored using a 3D flexural slip unfolding algorithm. As a key horizon for the Alpine tectonic restoration, we used the oldest post-rifting available horizon (i.e., the Aptian unconformity, the top of the Maiolica Fm.) that we assumed to be horizontal all across the study area. Finally, the syn-rift fault displacements were restored using a 3D simple shear un-faulting method (Withjack et al., 1995). The restored geometries were then compared to structural data from fault surfaces (results in Section 2.2). Finally, from the 3D geologic model, we derived an isopach 2D contour map, projected on the restored top of Middle Triassic surface.

Deleted: the Middle

3.2 Kinematic analysis

Kinematic data were collected along the early Permian-Middle Triassic fault systems to determine the orientation of the best-fit moment tensor solution, enabling to calculate the paleo-strain orientation for each tectonic phase. We calculated moment tensor summations of the strain axes (i.e., $E1 \geq E2 \geq E3$; extension positive), as implemented in FaultKin 8 (<http://www.geo.cornell.edu/geology/faculty/RWA/RWA.html>). For a complete discussion of the assumptions and limitations of these methods see Marrett and Allmendinger (1990). We inverted the fault slip data from their present-day orientation and, in order account for the later Alpine tectonics, we restored the obtained fault plane solution according to the bedding plane (S0), extrapolated from the nearest sector, along strike.

3.3 Thermochronology

3.3.1 Zircon (U-Th)/He dating

We collected samples from gneiss and micaschists of the Variscan basement in the hanging walls and footwalls of major faults. Zircon (U-Th)/He (ZHe) analysis was conducted at ETH Zurich. Zircon grains were first extracted from crushed samples using conventional methods of heavy liquid and magnetic separation. Euhedral zircons with widths of $>60 \mu\text{m}$ were then selected from each sample under a polarized stereo-microscope. Each grain was photographed to measure its dimensions for the calculation of alpha-ejection correction factor (FTK) following Ketcham et al. (2011). Afterwards, each zircon was packed in Niobium foil, and loaded into an ultra-high vacuum sample chamber. ^4He amounts were determined by outgassing with a diode laser at 1090°C for 45 minutes and measuring the released gas on a magnetic sector-field mass spectrometer equipped with a Baur-Singer ion source in static vacuum. A second extraction was conducted for each grain at 1110°C for 22 minutes. A third extraction was performed at 1130°C for 22 minutes for the grains, which still had high fractions of ^4He released from the second extraction ($>1\%$). Outgassed zircons were then transferred into Teflon vials, spiked with ^{233}U and ^{230}Th mixed solution, and dissolved first at 225°C for 72 hours in a concentrated mixture of HF and HNO_3 and then in concentrated HCl at 200°C for 24 hours to ensure dissolution of refractory fluoride salts. U and Th concentrations of each final solution were measured on an inductively coupled plasma mass spectrometer (ElementXR). To verify the accuracy of date estimates and monitor intrasample dispersion, six zircons from the Fish Canyon Tuff were processed alongside the samples. These zircons were not used for calibration purposes. They yielded a mean FTK age of $27.2 \pm 1.5 \text{ Ma}$ (\pm standard deviation (1s); supplementary material Table S2), which are consistent with the recommended eruption age of 28.0–28.2 Ma (Boehnke and Harrison, 2014).

3.3.2 Thermochronologic modelling

To evaluate the thermal effect related to the granitic intrusion occurring in the area, we calculated the heat transfer from the cooling granitic stock to the surrounding crust by means of a simple 1D transient diffusion equation. We assumed that the magmatic body emplacement occurred instantaneously and that the size of the stock was relatively small with respect to the

thickness of the intruded crust (Ehlers et al., 2003). With these conditions the temperature (T) of any point at a given distance
 220 from the intrusion (z) with time (t), is provided by Carslaw and Jaeger (1959):

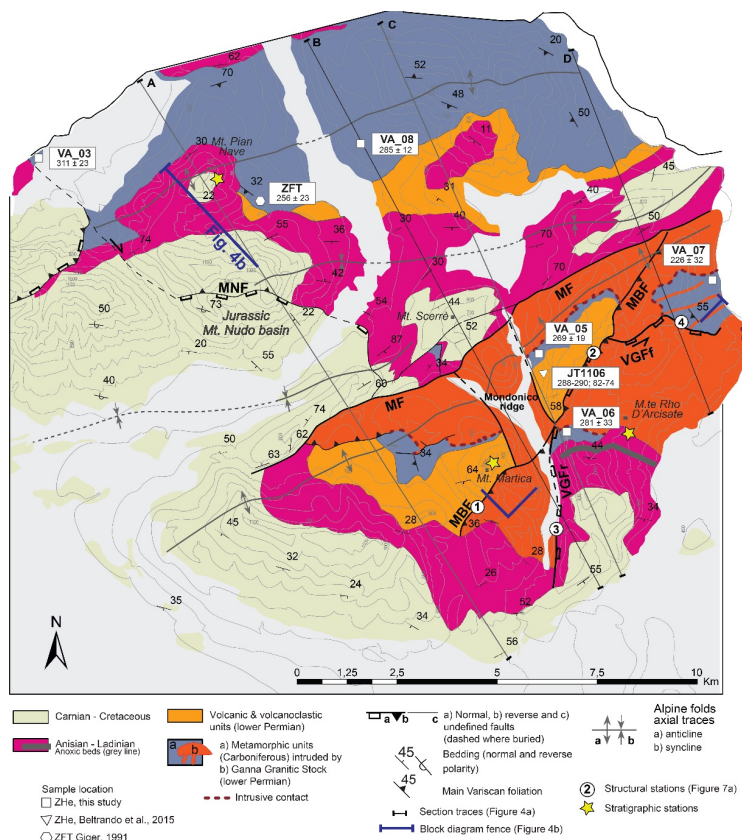
$$T(z,t) = T_b + \frac{T_i - T_b}{2} \left[\operatorname{erf} \left(\frac{L/2 - z}{2\sqrt{at}} \right) + \operatorname{erf} \left(\frac{L/2 + z}{2\sqrt{at}} \right) \right]$$

where T_i is the temperature of the intrusion, T_b the one of the crust, L is the intrusive body thickness, and a is the thermal
 225 conductivity coefficient. Erf is the error function (Abramowitz and Stegun, 1970).

4 Results

4.1 Tectono-Stratigraphy

The succession outcropping in the study area is comprised between the Carboniferous and the Cretaceous (Figure 3). We
 230 focused on the lower Permian-Middle Triassic succession as it records the transition between the Variscan and the Alpine
 cycles. Tectono-stratigraphic results are summarized in the following sections and illustrated in the geological map in Figure
 3 and in the sections and tectono-stratigraphic scheme of Figure 4.



235 **Figure 3: Geological map of the Study area (modified after Scaramuzzo et al., 2022). ZHe: zircon (U-Th)/He; ZFT: zircon fission-track. Fault codes: MF, Marzio Fault; MBF, Martica - Boarezzo Fault; VGFr, Valganna Fault ramp segment; VGfF, Valganna Fault flat segment. The Mt. Nudo basin is Jurassic in age (Kalin and Trumphy, 1977).**

4.1.1 The lower Permian succession

240 The lower Permian succession is composed of: i) the Ganna Granitic Stock, intruded at shallow levels within the Variscan basement, with its intrusive contacts exposed both at the top and at the base of the stock (Figures 3 and 4); and ii) the volcanic and volcano-clastic units, lying on top of the basement, above the Hercynian unconformity.

The lower Permian succession records the activity of the Marzio Fault. This is a near vertical structure that divides the study area into northern and southern blocks along a NE-SW direction (Figure 3). Stratigraphic sections measured on both sides of this fault (Figure 4b) show an abrupt increase in the thickness of the lower Permian volcanic/volcanoclastic rocks from approximately 200 m in the northern fault block to about 1500 m in the southern fault block (section A in Figure 4a, Figure 4b). This fault bounds sharply to the north also the lower Permian intrusive stock and puts it in contact with pre- to lower Permian, metamorphic and volcanic rocks (Figure 3; Figure 4a, b). Thin dikes and sills are commonly associated with the stock, cutting through the basement south of the Marzio Fault, whereas they are absent to the north of the Fault (Bernoulli et al., 2018). To the south of the Marzio Fault, the lower Permian intrusive and extrusive rocks are also displaced by a reverse fault that we here describe for the first time: namely, the Martica-Boarezzo Fault. This is a SW-NE striking, high-angle, SE-dipping fault. This structure displaces the Ganna Granitic Stock onto the lower Permian extrusive units (sections A and C, in Figure 4a) and abuts onto the Marzio Fault to the north-east (Figure 3).

The middle Permian Unconformity truncates the Martica-Boarezzo Fault (Figure 3 and Figure 4b). Thus, the age of the Martica-Boarezzo Fault is constrained between the late early Permian and the middle Permian.

South of the Marzio Fault and north of the Martica-Boarezzo Fault, two high-angle NNW-SSE trending faults bound a narrow structural high known as the Mondonico ridge (Figure 3). Due to erosion, no crosscut relationship with the stratigraphic succession exist to constrain the timing of the activity of the Mondonico ridge. While the faults bounding this ridge appear to be displaced by the Martica-Boarezzo Fault, evidence for this interpretation is limited due to the extensive coverage of Quaternary deposits. Alternatively, the development of the Mondonico ridge could have occurred contemporaneously with the activity of the Martica –Boarezzo Fault. Further research is required to investigate this hypothesis in greater depth.

Deleted: R

Deleted: of the

Deleted: Ridge

4.1.2 The Lower-Middle Triassic succession

On top of the middle Permian unconformity, thin, siliciclastic, Lower Triassic layers show no significant cross-cut relationship with the tectonic structures in the study area and are overlain by a thick carbonate succession that is Anisian-Ladinian in age.

This succession consists of platform and intra-platform facies with a highly variable distribution. In particular, the intraplatform facies (i.e., the anoxic beds within the Besano and Meride Formations) pinch out to the west. At the top, this succession is closed by an almost continuous interval with constant thickness, composed by thin bedded evaporitic dolostones of Carnian age (Pizzella Fm. in Figure 1).

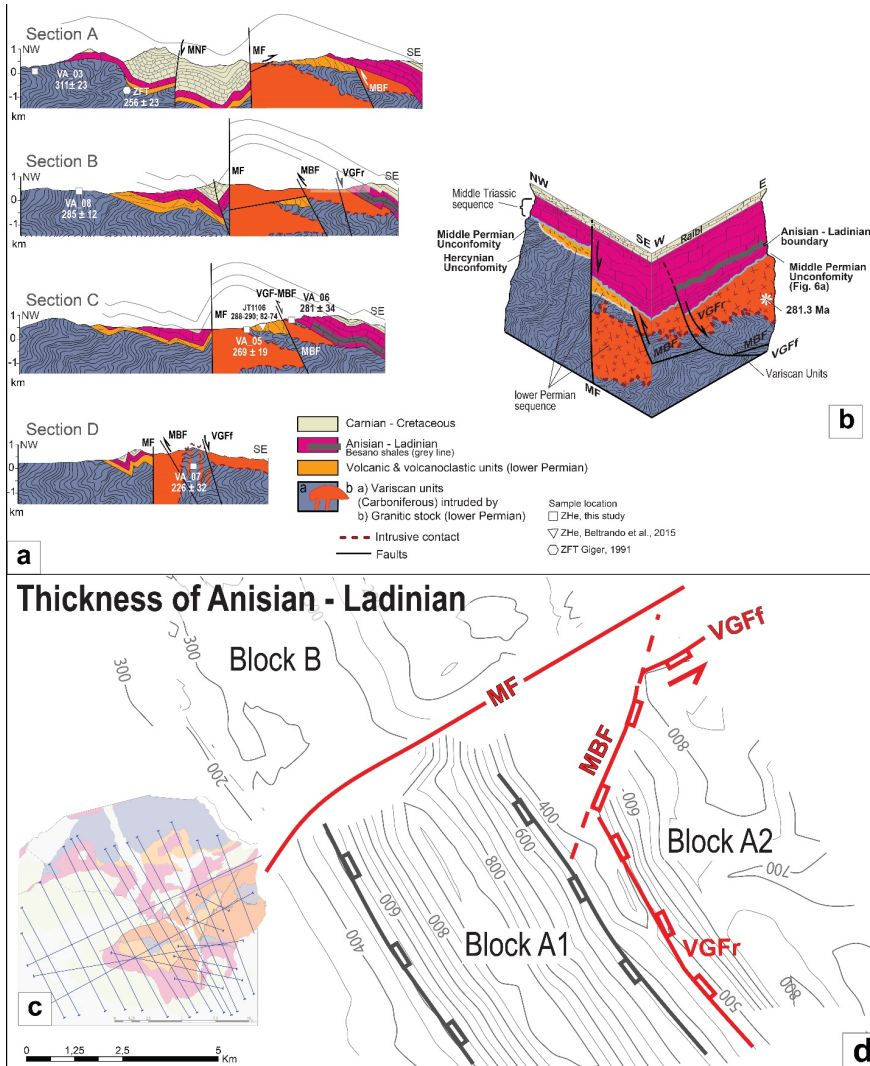
The Middle Triassic succession is gently folded or involved in Alpine thrusts north of the Marzio Fault, while, to the south, it is displaced by the Valganna Fault (Figure 3) with an apparent left-lateral separation. The Valganna Fault is limited to the hanging wall block of the Martica – Boarezzo fault, never displacing the latter and partly re-activating a small segment of the inherited reverse fault. The upper tip of the Valganna fault is sealed by the Carnian (Figure 3).

This structure is a normal fault presently describing an arcuate trace in map view due to Alpine tilting and erosion. Presently, the Valganna Fault is split into two segments with different orientation: a southern one, sub-vertical and striking N-S (VGFr in Figure 3 and sections B and C in Figure 4a), and a northern one, dipping ca. 60° with an ENE-WSW strike (VGFr in Figure

3, and section D in Figure 4a). If tilted back to their original attitude (S0 N170/40, measured ca. 1 km south of the VGFF), the two segments represent the shallow ramp (VGFr) and a slightly deeper, less steep sector (VGFF) of the Valganna Fault, respectively. The apparent left-lateral separation results from a combination of Alpine deformation and original Middle Triassic normal displacement. Specifically, after restoring and unfolding the Alpine deformation, a substantial residual normal offset remains along the Valganna Fault. The magnitude of this offset aligns with the thickness change that we measured across the fault. In fact, across VGFr, the Anisian–Ladinian succession shows a thickness increase [from 500 m to the east, up to 800 m, to the west](#) (sections B and C in Figure 4a and c). VGFF presently dips at a high angle to the SSE (sections C and D in Figure 4a) but its restored dip is close to 30°. It displaces the Ganna Granitic Stock, in the hanging wall, against the basement, in the footwall (Figure 3, section D in Figure 4a). At the junction between VGFF and VGFr, the Valganna Fault negatively inverts the inherited Martica–Boarezzo Fault. To the south, the Valganna Fault is clearly truncated by the top of the Anisian–Ladinian succession (Figure 3).

The Middle Triassic isopach map (Figure 4d) shows a variable basin topography in the study area. Differential subsidence, up to 600 m, occurs across the Marzio Fault between the northern block (block B in) and the more subsiding southern block (Block A in Figure 4d). The southern block features two narrows NW-SE elongated basins indicated as A1 and A2 in Figure 4d. The thickness analysis indicates that A1 and A2 are separated by a horst, are bounded by faults on the west and on the east and accommodated up to 800 m thick, Anisian–Ladinian sediments. The thickness analysis also suggests that the Valganna Fault bounds the eastern basin (A2) on the west and on the north, and the Marzio Fault bounds the western basin (A1) to the north.

Deleted: from 500 m,



300 Figure 4: a) Geological cross sections across the Study area; traces of the cross-sections in Figure 3. Codes: MBF, Martica-Boarezzo
Fault; MNF; Monte Nudo Fault; MF, Marzio Fault; VGF, Valganna Fault; b); ZHe: zircon (U-Th)/He; ZFT: zircon fission-track.
Tectono-stratigraphic block diagram of area (restored at Carnian); c) traces of the geological cross-sections' grid used to build the
3D geological model of the area; d) isopaches map of the Middle Triassic sequence (Anisian–Ladinian), after restoration, outcropping
faults are represented with red lines.

305

4.2 Fault kinematics and field evidence

In the field, the faults described in section 4.1 display the same crosscut relationship derived from mapping in several locations,
including still-preserved kinematic indicators.

310 We measured kinematic data i) along the Martica-Boarezzo Fault where it cuts through the Ganna Granitic Stocks and the
overlying Permian calc-alkaline succession (structural stations 1 and 2 in Figure 3), ii) along the Valganna Fault across the
Ladinian carbonate platform rocks, and iii) along the contact between the basement and the Ganna Granitic Stock (structural
stations 3 and 4 in Figure 3).

315 Along the Martica-Boarezzo Fault, fault steps and slickenlines indicate a reverse dip-slip sense of motion (Figure 5a, b) and
sets of P- and R-Riedel shears with related slickenlines that indicate right-lateral transpressive movements (Figure 5c, d). These
kinematic indicators are associated with syn-kinematic quartz veins and porphyric dikes (Figure 5c, e). At places, reverse faults
show evidence of a negative inversion, with overprinting steps and slickenlines, or a clear crosscut relationship with younger
normal faults, displacing the reverse ones (Figure 5c).

The inversion of fault-slip data (Figure 7b, c) indicates a strike slip to transpressive fault plane solution for the Martica-
Boarezzo fault, with a maximum shortening [axis](#) (i.e., strain axis E3) oriented ca. NW-SE (Figure 7b, c).

Deleted: axis (

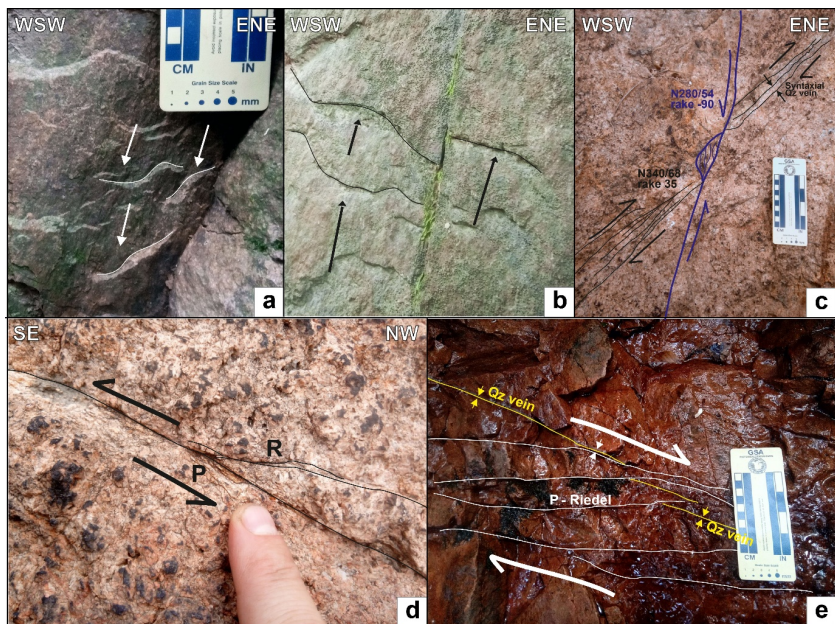


Figure 5: Representative kinematic features of the Martica-Boarezzo Fault; all the pictures are taken from the Ganna Granitic Stock, a) and b) hanging wall and footwall respectively high-angle reverse faults marked by fault steps and slickenlines; c) high-angle transpressive fault, associated with quartz veins and a thin quartz-porphyric dike, cut by a later high-angle normal fault (in blue); d) Left-lateral strike slip fault in the hanging wall of the MBT: note the associated R and P-fractures; e) Right-lateral strike slip fault : note the associated P-fractures and offset quartz veins.



Figure 6: a) middle Permian unconformity highlighted by the contact between the lower Permian Ganna Granitic Stock and the Anisian Bellano Fm.; b) detail of the base of the Bellano Fm.; c, d, e, f, mesoscopic structural features of Valganna Fault (c, d, e, f).

330

The Valganna Fault core is exposed locally, where it displaces the Anisian–Ladinian succession showing fault breccia to fault gauge up to ca. 10 m thick (Figure 6f), surrounded by a tens of meters wide discrete damage zone. Fault slip data along the Valganna Fault (Figure 7a) point to an extensional to slightly transtensional kinematics. High-angle, SE-dipping fault surfaces are most common along the ramp segment of the Valganna Fault, which features three sets of normal faults and strike-slip faults (Figure 7b). The slip inversion of these faults, after backfolding, indicates E-W extension (Figure 7c). Along the flat

335

segment of the Valganna Fault, two main sets of normal and transpressive faults (Figure 7a) indicate WNW-ESE directed extension, after backfolding (Figure 7b).

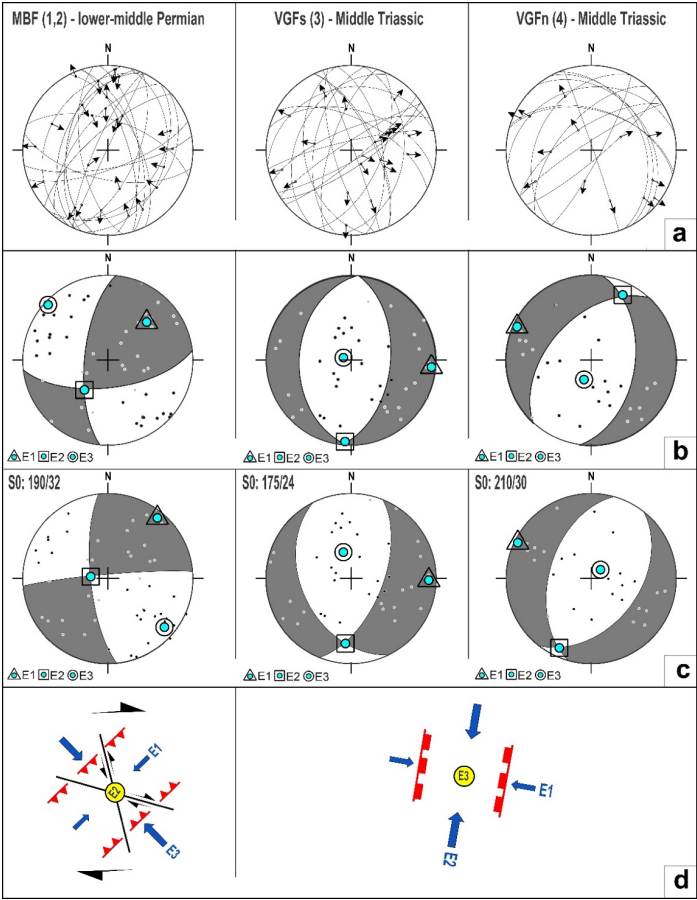


Figure 7: Fault slip data and inversion: a) fault slip data along the faults described in the text (see Figure 3 for the location of the structural stations); b) kinematic inversion, P and T axes and the best fit fault plane solutions are represented; c) kinematic inversion after restoration to the nearest bedding orientation (S0); Codes: MBF: Martica-Boarezzo Fault; VGFr: Valganna Fault – ramp segment; VGFF – Valganna Fault – flat segment; d) schematic diagrams summarizing the relationships between the orientations of strain axes and the strike a kinematics of expected fault.

345 **4.3 Thermochronology**

4.3.1 (U-Th)/He dates

Five samples, out of nine, from gneiss and micaschists provided good quality zircons for (U-Th)/He (ZHe) dating. Sample mean ages and their one standard deviations (1s) are given in Table 1 and reported both in the geological map (Figure 3) and in the geological cross-sections (Figure 4). Sample details are outlined in the Supplementary Table S2, presenting measured
350 quantities of U, Th, Sm, and He along with their uncertainties calculated from one standard deviation (1s) of the measurements. Additionally, the table includes single grain ages and their corresponding propagated measurement uncertainties (1s). Three samples (VA05, VA06, VA07) are in the hanging wall of the Marzio Fault close to the Ganna Granitic Stock, and two samples (VA03 and VA08) are from the block that acted as footwall of the Mt. Nudo Fault and of the Marzio Fault (Figure 2). One sample (VA07) includes 11 grains with a mean Late Triassic ZHe age of 226 ± 32 Ma (1s, 14%); three samples (VA05, 06,
355 and 08) include four to seven grains with mean ZHe ages in the range from 268 to 284 Ma, which is early Permian, and with standard deviations (1s) varying from 19 Ma to 34 Ma (from 4% to 12%); finally, one sample (VA03) with four grains gives a late Carboniferous age of 311 ± 23 Ma (1s, 7%).

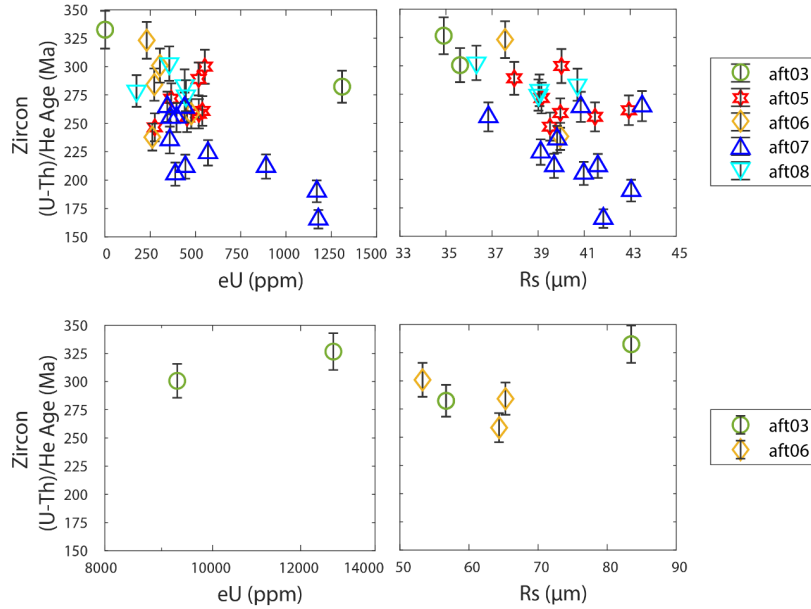


Figure 8: Diagram showing all zircons (U-Th)/He data plotted against effective uranium (Ue) concentrations and equivalent spherical radius (Rs). Uncertainties are one standard deviations.

The standard deviation of samples VA06 and VA07, 12% and 14%, respectively, is significantly higher than the 6% of the Fisch Canyon Tuff zircons, which were processed together with our samples. This observation suggests that samples VA06 and VA07 could be over-dispersed. Age dispersion can reflect either different zircon features like, for instance, differences in grain size, in radiation damage, and in U and Th distributions, or simply analytical uncertainties that cannot be accounted for.

Zircon dimensions control the size of the He diffusion domain and this results in positive correlations among ZHe closure temperature, zircon dimensions, and ZHe ages (e.g., Reiners and Brandon, 2006). The radiation damage accumulated in zircons also controls the closure temperature and, in turn, is controlled by the zircon U and Th concentrations and thermal history (Shuster et al., 2006). The effect of the radiation damage on the ZHe closure temperature is non-linear, and it can be identified by plotting ZHe ages against the effective U concentration (eU), which is a proxy for the radiation damage (Gautheron et al., 2009). Additionally, non-homogeneous U and Th distribution in zircon can result in an inaccurate alpha-ejection correction and in age dispersion (Hourigan et al., 2005). All these effects can occur at the same time making it difficult to separate them. In our samples, we did not correct for non-homogeneous U and Th distributions, as this would require additional, non-routine measurements. However, we observe a slight negative age-eU relationship in VA07 and no correlation with grain size in any

sample (Figure 8). Thus, the age overdispersion in VA06 and VA07 could relate partly to the effect of radiation damage and partly to other effects that we cannot account for.

Sample Code	Coordinates (Lat.; Long.) -WGS84	Elevation (m a.s.l.)	N. grains	Age (Ma)	Standard deviation 1 s (Ma)
VA03	45.956203°; 8.667739°	205	4	310.53	23.33
VA05	45.911899°; 8.830069°	563	7	268.82	19.32
VA06	45.892824°; 8.840748°	796	5	280.92	33.73
VA07	45.929817°; 8.886418°	358	11	225.74	32.38
VA08	45.956942°; 8.770584°	340	4	284.76	12.53

Table 1: Summary of (U-Th)/He age results; see Figure 1 for sample location on map and Figure 7 for locations in geological cross-sections.

We used the Welch t-test (Welch, 1947) to test whether our samples have equal ZHe mean ages: results (Table 2) indicate that the Triassic sample is younger than the other samples; the three early Permian samples have equal ZHe ages and the late Carboniferous sample has equal mean as two out of three of the early Permian samples and could be slightly older than the third sample.

		Triassic	Permian			Carboniferous
		VA07	VA05	VA06	VA08	VA03
Triassic	VA07	-	<0.05	<0.05	<0.05	<0.05
Permian	VA05		-	0.498	0.133	<0.05
	VA06			-	0.823	0.165
	VA08				-	0.114
Carboniferous	VA03					-

Table 2: t-test on the obtained (U-Th)/He ages to check the probability that two samples derive from two overlapping distributions sharing the same mean; Triassic ages highlighted in yellow, Permian in blue and Late Variscan in red, for ease of comparison.

4.3.2 The effect of the granitic intrusion onto the thermochronologic record

The proximity of some of our samples to a granitic intrusion, i.e., the Ganna Granitic stock, which is early Permian in age (281.3 ± 0.5 Ma; Schaltegger and Brack, 2007), suggests that post-magmatic cooling rather than cooling related to exhumation

could affect the ZHe ages. Three samples (VA05, VA06, and VA07) are very proximal (≤ 2 km away, Figure 3) to the Ganna granitic stock, whereas two samples (VA08 and VA03) are several kilometres from the intrusion, about 5 km and >10 km, respectively. Among the samples proximal to the intrusion, only two (VA05 and VA06) have ZHe ages similar to the intrusion age whereas one sample (VA07) has a Triassic ZHe age. The samples far from the intrusion (VA08 and VA03) have ZHe ages similar within uncertainty to the Ganna intrusion age.

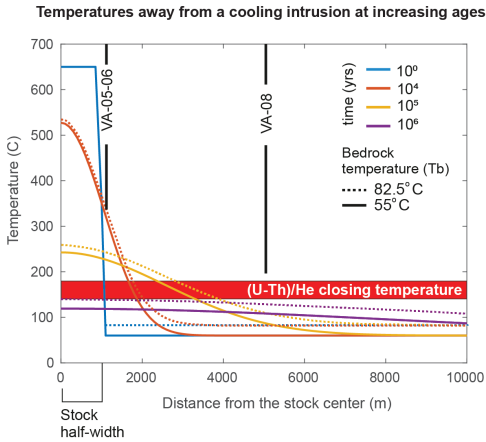


Figure 9: One dimensional transient thermal response to an intrusion (halfwidth = 1000 m). Intrusion depth was assumed to be shallow and into country rock at background temperature ranging between 55oC and 82.5oC.; initial intrusion temperature of 650 °C, and thermal diffusivity of 32 km²/Myr.

To test for the thermal effect related to the intrusion, we used a 1-D heat-transfer model at shallow depth combined with an estimate of the time-temperature conditions, at which a heating event could cause He loss in zircons. For the heat-transfer model, we assumed a background temperature ranging between 55 and 82.5 °C, consistent with a near-surface intrusion depth (i.e., less than 2 kbar; Bakos et al., 1990), an initial intrusion temperature of 650 °C and a thermal diffusivity of 32 km²/Myr (Figure 9). These inputs result in temperatures close to the intrusion temperature for 1 yr at a horizontal distance of 1 km from the granite and temperatures in the range of 200 °C and to 250 °C for 0.1 Ma at 2 km distance. To calculate how long a zircon should be held at a certain temperature to cause 90% He loss, which would cause age resetting, we used the partial loss-only He diffusion equations (Reiners and Brandon, 2006). In these equations we input average ZHe kinetic parameters (Reiners et al., 2004) and grain dimensions equal to the mean equivalent spherical radius (Rs; Supplementary Material Table S2) of the zircons dated in this study (Rs: 45 µm). We obtained that a steady temperature close to 400 °C for 1 yr results in 90% He loss whereas a steady temperature close to 200 °C requires at least 1 Ma time to produce 90% He loss. Thus, the early Permian

Deleted: In order to

410 ZHe ages of VA05 and VA06, which are proximal to the intrusion, likely reflect post-magmatic cooling. In contrast, the early
Permian ZHe ages of VA08 and VA03, located over 5 km from the intrusion, allow for two possible interpretations: they may
record cooling related to exhumation or reflect post-magmatic cooling related to a buried, unexposed granite in the footwall
of the Marzio Fault. Lastly, the cooling ages of VA07 span a range from 250 to 170 Ma -encompassing the timing of the Ganna
granitic intrusion but extending into the Middle Jurassic – too wide a span to solely reflect post-magmatic cooling.

415 **5 Discussion**

5.1.1 Permian thermal record

In the study area, previous thermochronologic data include a schist sample with a zircon fission-track age of 256 Ma (Giger,
1991) and a Permian volcanoclastic sample with two distinct ZHe age clusters: an older cluster between 288 Ma to 280 Ma
and a younger one between 82 and 74 Ma (Beltrando et al., 2015). The age clusters of this volcanoclastic sample indicate
420 Permian cooling, no rift-related He-loss, and possibly some early Alpine heating. Although this sample is close to one of ours,
we find no evidence of an Alpine thermal overprint in any of our samples, which collectively include 31 zircons. This suggests
that the Alpine thermal overprint may be restricted locally. The complex ZHe age distribution of the volcanoclastic sample
might also partially reflect its clastic nature, implying that the sample may include zircons with a long and varied geologic
history that respond diversely to low-T thermal events. In contrast, the simpler, narrowly dispersed ZHe age distributions in
425 our samples may relate to their origin in Carboniferous metamorphic rocks, which were likely metamorphosed at temperatures
sufficient to anneal the inherited histories of the zircons. Alternatively, the relatively limited age distribution in our samples
might reflect the small number of grains analysed per sample, potentially undersampling the full ZHe age distribution. [Overall,](#)
[our](#) samples exhibit little to no post-Permian rejuvenation: three out of the five samples have mean ZHe ages that are Permian,
while the remaining two samples are dated to the late Carboniferous and Late Triassic, respectively.

430 The Permian thermal record of several of our samples appears to be associated with the emplacement of the Ganna Granitic
Stock. Two Permian ZHe ages (VA05: 269±19 Ma; VA06: 281±33 Ma) from basement rocks south of the Marzio Fault were
thermally reset by this intrusion. These ages likely represent post-magmatic cooling, indicating that the Ganna Granitic Stock
intruded Carboniferous metamorphic rocks at 281 Ma. A third sample (VA07: 226±32) from nearby basement rocks has a
younger, more dispersed ZHe age range (260-170 Ma) with a negative relationship with eU (Figure 8), hinting at an additional
435 thermal event beyond the granitic intrusion. Thus, by the early-middle Permian, rocks south of the Marzio Fault were likely at
shallow crustal levels, at depths near or shallower than the ZHe closure temperature (i.e., ~180 °C; Reiners and Brandon, 2006).
North of the Marzio fault, two samples show Permian (VA08: 285±12 Ma) and late Carboniferous (VA03: 311±23 Ma) ZHe
ages. Despite being statistically similar (T-test, Table 2), VA08 aligns with the timing of the Ganna Granitic Stock intrusion.
A 1D thermal model indicates that the thermal effect of a shallowly emplaced granitic intrusion drops rapidly both in space
440 and time, and no field evidence suggests a granitic intrusion near VA08. While buried, unexposed granitic intrusions near
VA08 are possible, given the landscape's topography, with incised valleys, the likelihood of unexposed granites is minimal.

Deleted: Overall, our

Field data indicate that during the early-middle Permian, the Marzio fault acted as a normal fault with volcanic and magmatic activity in the hanging wall. Despite no thermochronologic age offset across the fault, our data are consistent with the normal activity of the Marzio fault during the early-middle Permian. The lack of offset likely reflects the thermal overprint from the granitic intrusion, which masked the typical cooling age pattern across a normal fault, where younger cooling ages would be normally observed in the footwall (e.g., Willett et al., 2021). In this context, VA08 and VA03 record exhumation of the footwall prior to and during the emplacement of the Ganna Granitic stock, while VA05, VA06 and VA07 were thermally reset by the intrusion. The slightly older Carboniferous age of VA03 may reflect its greater distance from the Marzio Fault, consistent with the trend of younger ages in footwall rocks closer to a fault. The younger cooling age of VA07 may relate to its lower elevation in the tectonic-stratigraphic succession of the study area, near the eastern margin. This margin is near the area affected by Late Triassic-Jurassic crustal thinning, generated by a widespread thermal anomaly that affected the thermochronologic record of the basement rocks of the central Southern Alps and resulting also in the emplacement of ore deposits (Bertotti et al., 1999; Giorno et al., 2022). The ZHe age distribution of VA07, along with its negative relationship with eU (Figure 8) suggests that this sample accumulated high radiation damage over a long residence at shallow crustal depths, with partial thermal rejuvenation possibly starting in the Triassic and persisting into the early Jurassic. Consequently, the Late Triassic-Jurassic thermal anomaly in the Southern Alps is evident only in sample VA07.

In conclusion, our thermochronologic data indicate that since the early Permian, basement rocks in the study area have been relatively stable, residing at shallow depths with minimal exposure to later thermal events. This long-term stability highlights a unique thermal history for the region, with most rocks undisturbed by major post-Permian thermal episodes, reinforcing a consistent, shallow-crustal preservation since the Permian.

Deleted: in

Deleted: one

Deleted: the events that occurred during

Deleted: constraining

Deleted: ,

Deleted: ,

Deleted: defining

Deleted: ¶

Deleted: ,

Deleted: ,

Deleted: While

Deleted: it is important to note that these variations could also reflect lateral changes in the thickness of the volcanic beds, the localized presence of lava domes, and the paleotopographic setting during the emplacement of the volcanic units (Di Capua et al., 2019). ¶

Further evidence highlights the Marzio Fault's structural control over the volcanic and magmatic activity during the Middle Permian. Thermochronologic data suggest exhumation of the Marzio Fault's footwall before and during the volcanic activity, aligning with its normal fault regime. Field observations from this and previous studies (Govi, 1960; Bakos et al., 1990; Bernoulli, 2018) support this interpretation showing that the Ganna Granitic Stock and associated dikes, which may intrude the overlying basement unit, are absent north of the Marzio Fault, suggesting magmatic activity was confined to its southern side. Although no early Permian magmatic activity is present north of the Marzio Fault, mantle-derived basic intrusions in the adjoining Ivrea-Verbano Zone to the west cut across the lower crust, linking early Permian magmatic activity in the Southern Alps to crustal thinning, asthenospheric upwelling and magmatic underplating (e.g., Shaltegger and Brack, 2007). Unlike the shallow crustal rocks of the Varese area, the Ivrea Verbano Zone's lower crustal rocks were exposed to the surface through stepwise exhumation and tilting from the Jurassic through the middle-late Miocene (e.g., Wolff et al., 2012) with minimal impact on the study area.

Our observations are consistent with previous studies and altogether they indicate that the early Permian extensional phase undoubtedly occurred after the end of the Variscan cycle throughout the peri-Variscan terrain including the central Mediterranean area, i.e., Tuscany, Corsica-Sardinia, Calabria and Atlas (Figure 10; e.g., Ziegler and Stampfli, 2001, Stampfli and Kozur, 2006; Cassinis et al., 2012; Cassinis et al., 2018; Ballèvre et al., 2020; Elter et al., 2020; Molli et al., 2020). Some Authors interpret this massive cal-alkaline magmatism as associated with the extension related to the back-arc opening of the Paleotethys subduction zone (e.g., Visonà, 1982, Lorenz and Nicholls, 1984; Stille and Buletti, 1987; Di Battistini et al., 1988; Finger and Steyrer, 1990, 1991; Bonin et al., 1993; Doglioni, 1995; Ziegler and Stampfli, 2001, Stampfli and Kozur, 2006). No reliable fault kinematic indicators are available in the study area to further characterize the stress orientation of the early Permian tectonic phase. Notably, the most reliable observations and datasets nearby, in this line, indicate that extensional detachment faults and pull-apart transtensional basins come with crustal thinning and high temperature-low pressure metamorphism widespread in all the Southalpine domain and the central Mediterranean area, i.e., Corsica, Sardinia, Calabria (e.g., Phol et al., 2018; Roda et al., 2019; Zanchi et al., 2019; Molli et al., 2020; Festa et al., 2022; Locchi et al., 2022). While a discussion regarding the geodynamic nature of the early Permian extensional phase may be somewhat speculative based on our data, our observations unequivocally show a lack of continuity between the early Permian rifting and the Mesozoic Alpine Tethys rifting (Figure 10). The early-middle Permian geologic record in our study area attests to the shifting from a rifting phase to a transcurrent phase and to the development of the middle Permian unconformity. Indeed, the activity of the Martica-Boarezzo fault and Mondonico ridge is consistent with the observation by Cadel et al. (1986) and Gretter et al. (2013) of folded lower Permian deposits in the central Southern Alps suggesting a middle Permian transcurrent tectonic regime, and with paleomagnetic (Muttoni et al. 2003, 2009) and stratigraphic data (Cassinis et al., 2012; Gretter et al., 2013; Cassinis et al., 2018;). To our knowledge, the Martica-Boarezzo fault and Mondonico ridge represent a direct observation of structures related to the middle Permian transcurrent phase testifying to a regional-scale significance of this event. Some studies suggested that at this time there was indeed a change in the plate configuration from Pangea A to Pangea B between Gondwana and Laurasia (Muttoni et al. 2003, 2009, and references therein). While other studies suggested that this transcurrent phase is related

Deleted: Additional

Deleted: observations

Deleted: support

Deleted: the significant structural influence of

Deleted: on the

Deleted:

Deleted: Bernoulli, 2018;

Deleted: further

Deleted: ,

Deleted: as

Deleted: .

Deleted: ¶

The Ganna Granitic Stock represent one of the near-surface and upper crustal intrusions of early Permian age that are concentrated in some realms along the Southern Alps (Figure 10). All these centres correspond to prominent centres of Permian volcanic activity, but only the adjoining sector of the Ivrea-Verbano Zone exposes the complete magmatic system which ranges from mantle derived basic intrusions into the lower crust, to coeval volcanic products to the surface (Shaltegger and Brack, 2007; Figure 10). The crustal structures exposed in the Ivrea-Verbano Zone shows that lower crust thinning is connected to magmatic underplating related to the rising asthenosphere and magmatic underplating (e.g., Shaltegger and Brack, 2007).

Deleted: ¶

Deleted: ; Karakas et al., 2019; Ballèvre et al., 2020

Deleted: pure-

Deleted: ¶

Deleted: compressional

Deleted: phase

Deleted: the first

Deleted: compressional

Deleted:

to a dextral megashear system that was active during the oblique subduction of the Paleotethys and the opening of the Neotethys ocean (e.g., Cassinis et al., 2012; Gretter et al., 2013; Cassinis et al., 2018; see Torsvik and Cocks, 2004 for a complete discussion). However, the discussion supported by our dataset does not favour either of the two hypotheses.

5.3 The Alpine Cycle inception

560 The end of the middle Permian transcurrent phase is marked by the onlap of the late Permian-Early Triassic siliciclastic wedge related to the marine ingression of the Paleo-Tethys from the east (Figure 10; e.g., Bernoulli, 2007) and it is followed by a renewed phase of extension that evolved through several stages. Early Triassic units are paraconcordant with the overlying Middle Triassic ones. The only evidence for an Early Triassic tectonic activity is coming out from barite rich veins, associated with hydrothermalism, which cut through the Lower Triassic and are sealed by the Middle Triassic, consistently with other

565 observations in the Southern Alps (e.g. Martin et al., 2017). During the first stage, in our study area, the Middle Triassic tectonostratigraphic data constrain a significant increase in subsidence that allowed the accommodation of up 800 m thick platform carbonate alternating with intraplateau basinal sediments. Subsidence was associated with E-W oriented extension that was controlled by the activity of the Valganna Fault and that resulted into the dissection of the depocenter into sub-basins. The brittle nature of the ramp and flat segments of the

570 Valganna fault suggests that extension at this time was distributed within the shallower zone of the upper crust. The Middle Triassic extensional phase has been interpreted as related to the far field effect of the Meliata-Maliac oceans (e.g., Castellarin et al., 1980; 1988; Ziegler and Stampfli; 2001; Stampfli et al.; 2002; Armienti et al., 2003; Zanetti et al., 2013, Beltrando et al., 2015) or as the onset of the Alpine-Tethys opening (e.g., De Min et al., 2020; Real et al., 2023). Finally, in the second stage, during the Late Triassic extension was associated to localized lithospheric normal faulting that

575 ultimately led to crustal thinning and break-up (e.g., Bertotti et al., 1993; Gaetani et al., 2010). In the Late Triassic-early Jurassic, extension continued with an E-W direction, but localized onto few master faults located outside our study area, both to the west (Mt. Nudo Basin; Figure 1) and to the east (Lombardian Basin; e.g., Bernoulli, 1964; Bertotti et al., 1993), where kilometre-thick syn-rift sequences are preserved.

To the east of our study area, the Late Triassic-Jurassic crustal thinning produced a widespread thermal anomaly that affected

580 the thermochronologic record of the basement rocks of the central Southern Alps and emplacement of ore deposits (Bertotti et al., 1999; Giorno et al., 2022). In our study area, the thermal overprint is evident in only one of our samples (VA07), situated in the easternmost region, at the lowest elevation, and within the deepest layers of the tectonic-stratigraphic sequence. Thus, altogether our data support the idea that the Ladinian-Carnian extensional phase predates crustal thinning that started in the Norian (e.g., Figure 10; Bertotti et al., 1993; Gaetani et al., 2010). In this view, deformation in the Ladinian-Carnian, was

585 rather distributed resulting in modest amount of extension concentrated within the upper crust (Figure 10; Mohn et al., 2010; 2011; 2012; Péron-Pinvidic et al., 2013; Naibof et al., 2017) whereas from the Norian extension localized along few lithospheric detachment faults and led to crustal thinning (Figure 10; Péron-Pinvidic et al., 2013; Naibof et al., 2017). The co-

Deleted: transpressional

axiality that we observed between the extensional events in the Ladinian-Carnian and the following ones supports the idea of a continuity of the geodynamic setting from the Middle Triassic through the Jurassic. This inference is concordant with the evolution of extension as proposed by previous studies in the central Southern Alps (e.g., Bertotti et al., 1993; Gaetani et al., 2010). This view is also supported by the geochemical data from magmatic rock in the Dolomites indicating that the Ladinian-Carnian magmatism in the eastern Southern Alps was related to the lithosphere thinning and mantle upwelling due to rifting events that ultimately caused the break-up in the Late Triassic-Early Jurassic (De Min et al., 2020).

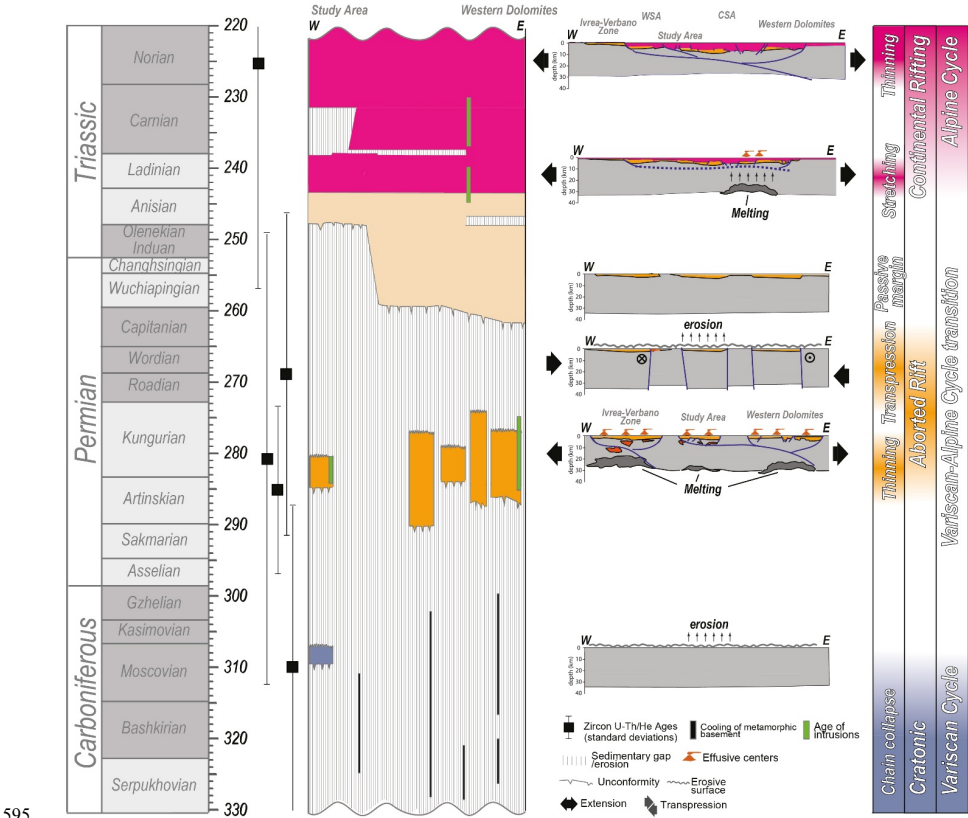


Figure 10. Conceptual and summary scheme of the Variscan-Alpine Cycle transition as constrained in this work and from other works (WSA, Western Southern Alps; CSA, Central Southern Alps): chronostratigraphic scheme redrawn after Schalteger and

Brack, 2007; Berra et al., 2009; Cassinis et al., 2012; Gretter et al., 2014; Beltrando et al., 2015; Cassinis et al., 2018; sections of the former Southern Alps redrawn after Beltrando et al., 2015.

7 Conclusions

This study provides new constraints on the Variscan-alpine cycle transition, a period relatively poorly documented within the European Southern Alps. Our data shed light on the transition from the early Permian rifting to the first inception of Triassic crustal extension, through a phase of transcurrent tectonics, previously undocumented in the study area.

In the framework of a regional perspective, the main findings of this work are:

- During the early Permian, a first rifting stage resulted in the accumulation of a thick pile of volcanic and volcanoclastic successions, deposited in a structurally controlled endorheic basin. At the same time, the emplacement of a fault-bounded intrusive stock at shallow depths caused the sudden heating of the surrounding basement rocks, followed by a later cooling at shallow crustal levels where they resided for the rest of their time.
- The sudden cessation of magmatic activity, followed by transcurrent tectonics (early p.p. – middle Permian) and a later regional-scale erosion (middle Permian), marks a distinct discontinuity in the regional Permo-Triassic evolution, that is the conclusion of a first cycle of crustal rifting and the shift toward the successive Alpine cycle.
- At the Middle Triassic, the inception of a second rifting event, here documented along a well-exposed normal fault, resulted in the exhumation of the fault footwall, as recorded by thermo-chronological dates, the subsidence of the fault hanging wall with drowning of the carbonate platform and development of a fault-bounded anoxic basin.
- It is suggested that the Middle Triassic extension could represent the stretching phase related to the onset of the Alpine Tethys rifting.

The main implications of our findings are that the onset of the Alpine cycle dates to the Middle Triassic and that there is no continuous Permo-Triassic extension, as previously suggested by other Authors (e.g., Winter and Bosellini, 1981), but there are multiple and distinct stages of rifting.

Appendices

Data availability

Fault slip data inversion were calculated using FaultKin v.8 software (<https://www.rickallmendinger.net/faultkin>) last accessed 03/04/2024). Thickness analyses were performed using the MOVE software (IPM v13.0 software suite, courtesy of Petroleum Experts Ltd). 3D mesh surfaces are available as 3D pdf file in supplementary material (S1). (U–Th)/He (ZHe) analysis results are available in the supplementary material Table S2 of this article. Geological map was done with QGIS 3.28.11 (<https://qgis.org/it/site/>) Last accessed 03/04/2024) and it is shown in Figure 3 of this article.

Deleted: In particular, our

Author contribution

Conceptualization: ES, FL, GF; Fieldwork and sample collection: ES, FL, Data collection: GF, CM; Data analysis: ES, FL, GF, CM; Methodology: ES, FL, GF, CM; Writing original draft: ES, FL, GF; Writing, review, and editing: ES, FL, GF, CM. All authors read and approved the final manuscript.

Competing interests

The authors declare that they have no conflict of interest.

Acknowledgements

ES and FL would like to thank A. Di Capua, M. Colombo their help with the fieldwork as well as fruitful consultations about the Permian volcanic evolution of the area. ES acknowledges P. Manzotti and M. Ballèvre for the discussions about Variscan-Permian evolution of the Alpine and central Europe area, and much more. We acknowledge A. Festa for commenting on an early version of this manuscript. We wish to thank three anonymous reviewers and Chris Morley for their constructive and helpful comments, and Federico Rossetti and Virginia Toy, for the editorial work.

Funding

This work benefited from funds from the PhD grant of Emanuele Scaramuzzo.

References

Abramowitz, M., and Stegun, I. (Eds.): Handbook of Mathematical Functions, Dover Publications, New York, USA, 1970.

Armienti, P., Corazzato, C., Groppelli, G., Natoli, E., and Pasquare, G.: Geological and petrographical study of Montecampione Triassic subvolcanic bodies (Southern Alps, Italy). Preliminary geodynamic results, Bollettino Della Società Geologica Italiana, 2, 67-78, 2003.

Baggio, P., and De Marco, L.: La serie basale tardo-paleozoica del Varesotto e le mineralizzazioni ad uranio della Valganna, Comitato nazionale per le ricerche nucleari – Studi Ricerche Divisione Geomineraria, 3, 15-103, 1960.

Bakos, F., Del Moro, A., and Visona, D.: The Hercynian volcano-phitonic association of Ganna (Lake Lugano, Central Southern Alps, Italy), European Journal of Mineralogy, 2, 373-384, <https://doi.org/10.1127/ejm/2/3/0373>, 1990.

Formatted: Font: Bold

Formatted: Font: Bold

Deleted: project

- Ballèvre, M., Camonin, A., Manzotti, P., and Poujol, M.: A step towards unraveling the paleogeographic attribution of pre-Mesozoic basement complexes in the Western Alps based on U–Pb geochronology of Permian magmatism, *Swiss Journal of Geosciences*, 113(1), 1-28, <https://doi.org/10.1186/s00015-020-00367-1>, 2020.
- Barth, S., Oberli, F., and Meier, M.: ThPb versus UPb isotope systematics in allanite from co-genetic rhyolite and granodiorite: Implications for geochronology, *Earth and Planetary Science Letters*, 124(1-4), 149-159, 1994.
- Beltrando, M., Stockli, D. F., Decarlis, A., and Manatschal, G.: A crustal-scale view at rift localization along the fossil Adriatic margin of the Alpine Tethys preserved in NW Italy, *Tectonics*, 34(9), 1927-1951, <https://doi.org/10.1002/2015TC003973>, 2015.
- Berger, A., Mercolli, I., Kapferer, N., and Fügenschuh, B.: Single and double exhumation of fault blocks in the internal Sesia-Lanzo Zone and the Ivrea-Verbano Zone (Biella, Italy), *International Journal of Earth Sciences*, 101(7), 1877-1894, <https://doi.org/10.1007/s00531-012-0755-6>, 2012.
- Bernoulli, D.: Zur Geologie des Monte Generoso (Lombardische Alpen); ein Beitrag zur Kenntnis der süd-alpinen Sedimente, *Beitr. Geol. Karte Schweiz*, N.F., 118, 1-134, 1964.
- Bernoulli, D.: The pre-Alpine geodynamic evolution of the Southern Alps: a short summary, *Bulletin für angewandte Geologie*, 12(2), 3-10, 2007.
- Bernoulli, D., Ambrosi, C., Scapozza, C., Stockar, R., and Schenker, F., Gaggero, L., Antognini, M. and Bronzini, S.: Foglio 1373 Mendrisio (parte Est) con parte Ovest del foglio Como. – Atlante geologico della Svizzera 1: 25 000, Note esplicative. In: Dall'Agnolo, Stephan, (ed.) Ufficio federale di topografia, CH- 3084 Wabern, Wabern. ISBN 978-3-302-40077-8, 2018
- Berra, F., Felletti, F., and Tesserollo, A.: Stratigraphic Architecture of a Transensional Continental Basin in Low-Latitude Semiarid Conditions: The Permian Succession of the Central Orobic Basin (Southern Alps, Italy), *Journal of Sedimentary Research*, 86(4), 408-429, <https://doi.org/10.2110/jsr.2016.26>, 2016.
- Berra, F., Galli, M. T., Reghellin, F., Torricelli, S., and Fantoni, R.: Stratigraphic evolution of the Triassic–Jurassic succession in the Western Southern Alps (Italy): the record of the two-stage rifting on the distal passive margin of Adria, *Basin Research*, 21(3), 335-353, <https://doi.org/10.1111/j.1365-2117.2008.00384.x>, 2009.

- Berra, F., Tiepolo, M., Caironi, V., and Siletto, G. B.: U–Pb zircon geochronology of volcanic deposits from the Permian basin of the Orobic Alps (Southern Alps, Lombardy): chronostratigraphic and geological implications, *Geological Magazine*, 152(3), 429–443, <https://doi.org/10.1017/S0016756814000405>, 2015.
- 695 Bertotti, G., Picotti, V., Bernoulli, D., and Castellarin, A.: From rifting to drifting: tectonic evolution of the South-Alpine upper crust from the Triassic to the Early Cretaceous, *Sedimentary Geology*, 86(1-2), 53–76, [https://doi.org/10.1016/0037-0738\(93\)90133-P](https://doi.org/10.1016/0037-0738(93)90133-P), 1993.
- Bertotti, G., Seward, D., Wijbrans, J., Ter Voorde, M., and Hurford, A. J.: Crustal thermal regime prior to, during, and after rifting: A geochronological and modeling study of the Mesozoic South Alpine rifted margin, *Tectonics*, 18(2), 185–200, <https://doi.org/10.1029/1998TC900028>, 1999.
- 700 Bigi, G., Cosentino, D., Parotto, M., Sartori, R., and Scandone, P.: Structural Model of Italy Scale 1: 500.000—Consiglio Nazionale delle Ricerche—Progetto Finalizzato Geodinamica. SELCA, Firenze, Italy, 1992.
- 705 Boehnke, P., and Harrison, T. M.: A meta-analysis of geochronologically relevant half-lives: what’s the best decay constant?, *International Geology Review*, 56(7), 905–914, <https://doi.org/10.1080/00206814.2014.908420>, 2014.
- Bonin, B., Brandlein, P., Bussy, F., Desmons, J., Eggenberger, U., Finger, F., Graf, K., Marro, C., Mercogli, I., Oberhänsli, R., Ploquin, A., Quadt von, A., Raumer von, J., Schaltegger, U., Steyrer, H.P., Vison’a, D., and Vivier, G.: Late Variscan Magmatic Evolution of the Alpine Basement, in: *The pre-Mesozoic Geology in the Alps*, edited by: von Raumer, J., and Neubauer, F., Springer, Berlin, Germany, 169–199, 1993.
- 710 Boriani, A., Burlini, L., and Sacchi, R.: The Cossato-Mergozzo-Brissago Line and the Pogallo Line (Southern Alps, Northern Italy) and their relationships with the late-Hercynian magmatic and metamorphic events, *Tectonophysics*, 182(1-2), 91–102, [https://doi.org/10.1016/0040-1951\(90\)90344-8](https://doi.org/10.1016/0040-1951(90)90344-8), 1990.
- 715 Boriani, A., Sassi, F., and Sassi, R.: The basement complexes in Italy, with special regards to those exposed in the Alps: a review, *Episodes*, 26(3), 186–192, <https://doi.org/10.18814/epiiugs/2003/v26i3/006>, 2003.
- Boriani, A., and Villa, I. M.: Geochronology of regional metamorphism in the Ivrea-Verbano zone and Serie dei Laghi, Italian Alps, *Schweizerische Mineralogische und Petrographische Mitteilungen*, 77, 381–401, 1997.
- 720 Brack, P., and Rieber, H.: Towards a better definition of the Anisian/Ladinian boundary: New biostratigraphic data and correlations of boundary sections from the Southern Alps, *Eclogae Geologicae Helvetiae*, 86(2), 415–527, 1993.

725 Cadel, G.: Geology and uranium mineralization of the Collio Basin (central Southern Alps, Italy), *Uranium*, 2(3), 215-240, 1986.

Carraro, F., and Ferrara, G.: Alpine “Tonalite” at Miagliano, Biella (Zona Diorito-Kinzigitica). A preliminary note, *Schweizerische Mineralogische Petrographische Mitteilungen*, 48, 75-80, 1968.

730 Carslaw, H., and Jaeger, J.: *Conduction of Heat in Solids*, Clarendon Press, Oxford, United Kingdom, 510 pp., 1959.

Casati, P.: Tettonismo e sedimentazione nel settore occidentale delle Alpi Meridionali durante il tardo Paleozoico, il Triassico e il Giurassico, *Riv. ital. Paleontologia Stratigrafia*, 84, 313–326, 1978.

735 Cassinis, G., Perotti, C. R., and Ronchi, A.: Permian continental basins in the Southern Alps (Italy) and peri-mediterranean correlations, *International Journal of Earth Sciences*, 101(1), 129-157, <https://doi.org/10.1007/s00531-011-0642-6>, 2012.

Cassinis, G., Perotti, C., and Santi, G. Post-Variscan Verrucano-like deposits in Italy, and the onset of the alpine tectono-sedimentary cycle, *Earth-Science Reviews*, 185, 476-497, 2018.

740 Castellarin, A., Lucchini, F., Rossi, P.L., Selli, L., and Simboli, G.: The Middle Triassic magmatic-tectonic arc development in the Southern Alps, *Tectonophysics*, 146, 79-89, 1988.

De Min, A., Velicogna, M., Ziberna, L., Chiaradia, M., Alberti, A., and Marzoli, A.: Triassic magmatism in the European Southern Alps as an early phase of Pangea break-up, *Geological Magazine*, 157(11), 1800-1822, <https://doi.org/10.1017/S0016756820000084>, 2020.

745 Di Battistini, G., Bargossi, G. M., Spotti, G., and Toscani, L.: Andesites of the late Hercynian volcanic sequence in Trentino Alto Adige (Northern Italy), *Rendiconti Società Italiana Mineralogia Petrologia*, 43, 1087-1100, 1988.

750 [Di Capua, A. D., Scaramuzzo, E., Todaro, A., and Livio, F.: Permian volcanic and volcanoclastic sequences in the Varese area \(Northern Italy\): geometries, emplacement mechanisms and sediment supply of a volcanically controlled continental environment, *Geophysical Research Abstracts*, 21, 2019.](#)

755 Di Paola, S., Spalla, M. I., and Gosso, G.: New structural mapping and metamorphic evolution of the Domaso Cortafo Zone (Southern Alps-Lake Como), *Memorie di Scienze Geologiche*, Padova, 53, 1-14, 2001.

Formatted: English (UK)

Formatted: English (UK)

Formatted: English (UK)

Formatted: English (UK)

Formatted: English (UK)

Formatted: English (UK)

- Diella, V., Spalla, M. I., and Tunesi, A.: Contrasting thermomechanical evolutions in the Southalpine metamorphic basement of the Orobic Alps (Central Alps, Italy), *Journal of Metamorphic Geology*, 10(2), 203-219, <https://doi.org/10.1111/j.1525-1314.1992.tb00079.x>, 1992.
- Doglioni, C.: Geological remarks on the relationships between extension and convergent geodynamic settings, *Tectonophysics*, 252(1-4), 253-267, [https://doi.org/10.1016/0040-1951\(95\)00087-9](https://doi.org/10.1016/0040-1951(95)00087-9), 1995.
- Ehlers, T. A., Willett, S. D., Armstrong, P. A., and Chapman, D. S.: Exhumation of the central Wasatch Mountains, Utah: 2. Thermokinematic model of exhumation, erosion, and thermochronometer interpretation, *Journal of Geophysical Research: Solid Earth*, 108(B3), <https://doi.org/10.1029/2001JB001723>, 2003.
- Elter, F. M., Gaggero, L., Mantovani, F., Pandeli, E., and Costamagna, L. G. . The Atlas-East Variscan-Elbe shear system and its role in the formation of the pull-apart Late Palaeozoic basins. *International Journal of Earth Sciences*, 109, 739-760. <https://doi.org/10.1007/s00531-020-01830-y>, 2020.
- Ferrando, S., Bernoulli, D., & Compagnoni, R.: The Canavese zone (internal Western Alps): a distal margin of Adria, *Schweizerische Mineralogische und Petrographische Mitteilungen*, 84(1-20), 237-259, 2004.
- Festa, A., Balestro, G., Borghi, A., De Caroli, S., and Succo, A., The role of structural inheritance in continental break-up and exhumation of Alpine Tethyan mantle (Canavese Zone, Western Alps), *Geoscience Frontiers*, 11(1), 167-188, <https://doi.org/10.1016/j.gsf.2018.11.007>, 2020.
- Finger, F., and Steyrer, H.P.: I-type granitoids as indicators of a late Paleozoic convergent ocean–continent margin along the southern flank of the central European Variscan orogen, *Geology*, 18, 1207–1210, 1990.
- Finger, F., and Steyrer, H.P.: Comments and Replies on I-type granitoids as indicators of a late Paleozoic convergent ocean–continent margin along the southern flank of the central European Variscan orogen, *Geology* 19, 1245–1248, 1991.
- Furrer, H.: The Kalkschieferzone (Upper Meride Limestone; Ladinian) near Meride (Canton Ticino, Southern Switzerland) and the evolution of a Middle Triassic intraplateau basin, *Eclogae Geologicae Helvetiae*, 88, 827-852, 1995.
- Gaetani, M.: From Permian to Cretaceous: Adria as pivotal between extensions and rotations of Tethys and Atlantic Oceans, *Journal of the virtual explorer*, 36 (6), 3-46, <https://doi.org/10.3809/jvirtex.2010.00235>, 2010.

Formatted: English (US)

Formatted: English (US)

- Gaetani, M., Gnaccolini, M., Jadoul, F., and Garzanti, E.: Multiorder sequence stratigraphy in the Triassic system of the western Southern Alps: Mesozoic and Cenozoic sequence stratigraphy of European basins, *SEPM Special Publications*, 60, 701-717, 1998.
- 795 Gautheron, C., Tassan-Got, L., Barbarand, J., and Pagel, M.: Effect of alpha-damage annealing on apatite (U-Th)/He thermochronology, *Chemical Geology*, 266(3-4), 157-170, <https://doi.org/10.1016/j.chemgeo.2009.06.001>, 2009.
- Giger, M.: Geochronologische und petrographische Studien an Geröllen und Sedimenten der Gonfolite Lombarda Gruppe (Südschweiz und Norditalien) und ihr Vergleich mit dem alpinen Hinterland, Doctoral dissertation, University of Bern, Bern, Switzerland, 227 pp., 1991.
- 800
- Giorno, M., Barale, L., Bertok, C., Frenzel, M., Looser, N., Guillong, M., Bernasconi, S., and Martire, L.: Sulfide-associated hydrothermal dolomite and calcite reveal a shallow burial depth for Alpine-type Zn-(Pb) deposits, *Geology*, 50 (7), 853-858, <https://doi.org/10.1130/G49812.1>, 2022.
- 805
- Govi, M: *Geologia del territorio compreso tra il Lago di Lugano e la Val Marchirolo*, Studi e Ricerche della Divisione Geomineraria del CNR, 3, 160-217, 1960.
- Gretter, N., Ronchi, A., Langone, A., and Perotti, C. R.: The transition between the two major Permian tectono-stratigraphic cycles in the central Southern Alps: results from facies analysis and U/Pb geochronology, *International Journal of Earth Sciences*, 102(5), 1181-1202, <https://doi.org/10.1007/s00531-013-0886-4>, 2013.
- 810
- Handy, M. R., Franz, L., Heller, F., Janott, B., and Zurbiggen, R.: Multistage accretion and exhumation of the continental crust (Ivrea crustal section, Italy and Switzerland), *Tectonics*, 18(6), 1154-1177, <https://doi.org/10.1029/1999TC900034>, 1999.
- 815
- Heberer, B., Reverman, R. L., Fellin, M. G., Neubauer, F., Dunkl, I., Zattin, M., Seward, D., Genser, J., and Brack, P.: Postcollisional cooling history of the Eastern and Southern Alps and its linkage to Adria indentation, *International Journal of Earth Sciences*, 106(5), 1557-1580, <https://doi.org/10.1007/s00531-016-1367-3>, 2016.
- 820
- Hourigan, J. K., Reiners, P. W., and Brandon, M. T.: U-Th zonation-dependent alpha-ejection in (U-Th)/He chronometry, *Geochimica et Cosmochimica Acta*, 69(13), 3349-3365, <https://doi.org/10.1016/j.gca.2005.01.024>, 2005.
- Hunziker, J. C.: Rb-Sr and K-Ar age determination and the Alpine tectonic history of the Western Alps, *Mem. Ist. Geol. Mineral. Univ. Padova*, 31, 5-55, 1974.

- 825 Hurford, A. J.: Cooling and uplift patterns in the Lepontine Alps South Central Switzerland and an age of vertical movement on the Insubric fault line, *Contributions to mineralogy and petrology*, 92(4), 413–427, 1986.
- Jäger, E., and Faul, H., Altersbestimmungen an einigen Schweizer Gesteinen und dem Granit von Baveno, *Schweizerische Mineralogische und Petrographische Mitteilungen*, 40, 10–12, 1960.
- 830 Jongmans, W. J., and Ritter, E.: Die Karbonflora der Schweiz, *Beiträge zur geologischen Karte der Schweiz*, Kümmerly und Frey, 116 pp., 1960.
- 835 Kalin, O., and Trümpy, D.: Sedimentation und Palaotektonik in den westlichen Sudalpen: Zur triasisch-jurassischen Geschichte des Monte Nudo-Beckens, *Eclogae Geologicae Helvetiae*, 70, 295–350, 1960.
- Karakas, O., Wotzlaw, J. F., Guillong, M., Ulmer, P., Brack, P., Economos, R., Bergantz G. W., Sinigoi, S., and Bachmann, O.: The pace of crustal-scale magma accretion and differentiation beneath silicic caldera volcanoes, *Geology*, 47(8), 719–723, 840 <https://doi.org/10.1130/G46020.1>, 2019.
- Ketcahm, R.A., Gautheron, C., and Tassan-Got, L.: Accounting for long alpha-particle stopping distances in (U–Th–Sm)/He geochronology: Refinement of the baseline case, *Geochimica et Cosmochimica Acta*, 75, 7779–7791, 845 <https://doi.org/10.1016/j.gca.2011.10.011>, 2011.
- Locchi, S., Zanchetta, S., and Zanchi, A.: Evidence of Early Permian extension during the post-Variscan evolution of the central Southern Alps (N Italy), *International Journal of Earth Sciences*, 111(6), 1717–1738. <https://doi.org/10.1007/s00531-022-02220-2>, 2022.
- 850 Lorenz, V., and Nicholls, I. A.: Plate and intraplate processes of Hercynian Europe during the Late Paleozoic, *Tectonophysics*, 107(1–2), 25–56, 1984.
- Malavieille, J., Guihot, P., Costa, S., Lardeaux, J. M., and Gardien, V.: Collapse of the thickened Variscan crust in the French Massif Central: Mont Pilat extensional shear zone and St. Etienne Late Carboniferous basin, *Tectonophysics*, 177(1–3), 139– 855 149, 1990.
- Marocchi, M., Morelli, C., Mair, V., Klötzli, U. and Bargossi, G.M.: Evolution of Large Silicic Magma Systems: New U–Pb Zircon Data on the NW Permian Athesian Volcanic Group (Southern Alps, Italy), *Journal of Geology*, 116, 480–498, 2008.

- 860 Marrett, R., and Allmendinger, R. W.: Kinematic analysis of fault-slip data, *Journal of structural geology*, 12(8), 973-986, 1990.
- Martin, S., Bigazzi, G., Zattin, M., Viola, G., and Balestrieri, M. L.: Neogene kinematics of the Giudicarie fault (Central-Eastern Alps, Italy): new apatite fission-track data, *Terra Nova*, 10(4), 217-221, 1998.
- 865 Martin, S., Toffolo, L., Moroni, M., Montorfano, C., Secco, L., Agnini, C., Nimis, P., and Tumati, S.: Siderite deposits in northern Italy: Early Permian to Early Triassic hydrothermalism in the Southern Alps, *Lithos*, 284-285, 276-295, <https://doi.org/10.1016/j.lithos.2017.04.002>, 2017.
- 870 McDowell, F. W.: Potassium-argon ages from the Ceneri zone, Southern Swiss Alps, *Contributions to Mineralogy and Petrology*, 28(2), 165-182, 1970.
- McDowell, F. W., and Schmid, R.: Potassium-argon ages from the Valle d'Ossola section of the Ivrea-Verbano zone (northern Italy), *Schweizerische Mineralogische und Petrographische Mitteilungen*, 48, 205-210, 1968.
- 875 Mohn, G., Manatschal, G., Beltrando, M., Masini, E., and Kuszniir, N.: Necking of continental crust in magma-poor rifted margins: Evidence from the fossil Alpine Tethys margins, *Tectonics*, 31(1), TC1012, 2012.
- Mohn, G., Manatschal, G., Masini, E., and Müntener, O.: Rift-related inheritance in orogens: a case study from the 880 Austroalpine nappes in Central Alps (SE-Switzerland and N-Italy), *International Journal of Earth Sciences*, 100, 937-961, 2011.
- Molli, G., Brogi, A., Caggianelli, A., Capezzuoli, E., Liotta, D., Spina, A., and Zibra, I. Late Palaeozoic tectonics in Central Mediterranean: a reappraisal. *Swiss Journal of Geosciences*, 113, 1-32. <https://doi.org/10.1186/s00015-020-00375-1>. 2020
- 885 Mohn, G., Manatschal, G., Müntener, O., Beltrando, M., and Masini, E.: Unravelling the interaction between tectonic and sedimentary processes during lithospheric thinning in the Alpine Tethys margins, *International Journal of Earth Sciences*, 99, 75-101, 2010.
- Muttoni, G., Gaetani, M., Kent, D. V., Sciunnach, D., Angiolini, L., Berra, F., Garzanti, E., Mattei, M., and Zanchi, A.: Opening 890 of the Neo-Tethys Ocean and the Pangea B to Pangea A transformation during the Permian, *GeoArabia*, 14(4), 17-48, <https://doi.org/10.2113/geoarabia140417>, 2009.

- 895 Muttoni, G., Kent, D. V., Garzanti, E., Brack, P., Abrahamsen, N., and Gaetani, M.: Early Permian Pangea 'B' to Late Permian Pangea 'A', *Earth and Planetary Science Letters*, 215(3-4), 379-394, [https://doi.org/10.1016/S0012-821X\(03\)00452-7](https://doi.org/10.1016/S0012-821X(03)00452-7), 2003.
- Naliboff, J. B., Buiter, S. J., Péron-Pinvidic, G., Osmundsen, P. T., and Tetreault, J.: Complex fault interaction controls continental rifting, *Nature communications*, 8(1), 1179, <https://doi.org/10.1038/s41467-017-00904-x>, 2017.
- 900 Pohl, F., Froitzheim, N., Obermüller, G., Tomaschek, F., Schröder, O., Nagel, T. J., Schiunnach, D., and Heuser, A.: Kinematics and age of syn-intrusive detachment faulting in the Southern Alps: Evidence for Early Permian crustal extension and implications for the Pangea A versus B Controversy, *Tectonics*, 37(10), 3668-3689, <https://doi.org/10.1029/2018TC004974>, 2018,
- 905 Pomella, H., Stipp, M., and Fügenschuh, B.: Thermochronological record of thrusting and strike-slip faulting along the Giudicarie fault system (Alps, Northern Italy), *Tectonophysics*, 579, 118-130, <https://doi.org/10.1016/J.Tecto.2012.04.015>, 2012.
- Quick, J. E., Sinigoi, S., Peressini, G., Demarchi, G., Wooden, J. L., and Sbisà, A.: Magmatic plumbing of a large Permian caldera exposed to a depth of 25 km, *Geology*, 37(7), 603-606, 2009.
- 910 Real, C., Fassmer, K., Carosi, R., Froitzheim, N., Rubatto, D., Groppo, C., Münker, C., and Ferrando, S.: Carboniferous–Triassic tectonic and thermal evolution of the middle crust section of the Dervio–Olgiasca Zone (Southern Alps), *Journal of Metamorphic Geology*, 41(5), 685-718. <https://doi.org/10.1111/jmg.12714>, 2023.
- 915 Reiners, P. W., and Brandon, M. T.: Using thermochronology to understand orogenic erosion, *Annual Review of Earth and Planetary Sciences*, 34(1), 419-466, <https://doi.org/10.1146/annurev.earth.34.031405.125202>, 2006.
- Reiners, P. W., Spell, T. L., Nicolescu, S., and Zanetti, K. A.: Zircon (U-Th)/He thermochronometry: He diffusion and comparisons with $^{40}\text{Ar}/^{39}\text{Ar}$ dating, *Geochimica et cosmochimica acta*, 68(8), 1857-1887. <https://doi.org/10.1016/j.gca.2003.10.021>, 2004.
- 920 Renesto, S., and Stockar, R.: First record of a coelacanth fish from the Middle Triassic Meride Limestone of Monte San Giorgio (Canton Ticino, Switzerland), *Rivista Italiana di Paleontologia e Stratigrafia*, 124(3), 639-653, 2018.

Formatted

- 925 Reverman, R. L., Fellin, M. G., Herman, F., Willett, S. D., and Fitoussi, C.: Climatically versus tectonically forced erosion in the Alps: Thermochronometric constraints from the Adamello Complex, Southern Alps, Italy, *Earth and Planetary Science Letters*, 339, 127-138, <https://doi.org/10.1016/j.epsl.2012.04.051>, 2012.
- Roda, M., Regorda, A., Spalla, M. I., and Marotta, A. M.: What drives Alpine Tethys opening? Clues from the review of geological data and model predictions, *Geological Journal*, 54(4), 2646-2664, <https://doi.org/10.1002/gj.3316>, 2019.
- 930 Rosenberg, C. L., and Kissling, E.: Three-dimensional insight into Central-Alpine collision: Lower-plate or upper-plate indentation?, *Geology*, 41(12), 1219-1222, <https://doi.org/10.1130/G34584.1>, 2013.
- Scaramuzzo, E., Livio, F. A., Granado, P., Di Capua, A., and Bitonte, R.: Anatomy and kinematic evolution of an ancient passive margin involved into an orogenic wedge (Western Southern Alps, Varese area, Italy and Switzerland), *Swiss Journal of Geosciences*, 115(1), 1-21, <https://doi.org/10.1186/s00015-021-00404-7>, 2022.
- Schaltegger, U., and Brack, P.: Crustal-scale magmatic systems during intracontinental strike-slip tectonics: U, Pb and Hf isotopic constraints from Permian magmatic rocks of the Southern Alps, *International Journal of Earth Sciences*, 96(6), 1131-1151, <https://doi.org/10.1007/s00531-006-0165-8>, 2007.
- 940 Shuster, D. L., Flowers, R. M., and Farley, K. A.: The influence of natural radiation damage on helium diffusion kinetics in apatite, *Earth and Planetary Science Letters*, 249(3-4), 148-161, <https://doi.org/doi:10.1016/j.gca.2008.10.013>, 2006.
- 945 Siegesmund, S., Layer, P., Dunkl, I., Vollbrecht, A., Steenken, A., Wemmer, K., and Ahrendt, H.: Exhumation and deformation history of the lower crustal section of the Valstrona di Omegna in the Ivrea Zone, southern Alps, *Geological Society, London, Special Publications*, 298(1), 45-68, <https://doi.org/10.1144/SP298.3>, 2008.
- 950 Siletto, G. B., Spalla, M. I., Tunesi, A., Lardeaux, J. M., and Colombo, A. (1993). Pre-Alpine structural and metamorphic histories in the Orobic Southern Alps, Italy, in: *Pre-Mesozoic geology in the Alps*, edited by: Von Raumer, J. F., and Neubauer, F., Springer, Berlin, Germany, 585-598.
- Spalla, M. I., Diella, V., Pigazzini, N., Siletto, G. B., and Gosso, G.: Significato tettonico della transizione Cld-And nelle metapeliti del Basamento Sudalpino (Alta Val Camonica), *Rendiconti della Società Geologica Italiana*, 2, 182-183, 2006.
- 955 Stampfli, G. M.: The Intra-Alpine terrain: a Paleotethyan remnant in the Alpine Variscides, *Eclogae Geologicae Helveticae*, 89, 13-42, 1996.

- Stampfli, G. M.: Tethyan oceans, in: *Tectonics and Magmatism in Turkey and Surrounding Area*, edited by: Bozkurt, E.,
 960 Winchester, J. A. and Piper, J. D. A., Geological Society, London, Special Publications, 173, 1–23, 2000.
- Stampfli, G. M., and Kozur, H. W.: Europe from the Variscan to the Alpine cycles, in: *European Lithosphere Dynamics*, edited
 by: Gee, D. G., and Stephenson, R. A., Geological Society, London, Memoirs, 32(1), 57-82,
 10.1144/GSL.MEM.2006.032.01.04, 2006.
- 965 Stille, P., and Buletto, M.: Nd-Sr isotopic characteristics of the Lugano volcanic rocks and constraints on the continental crust
 formation in the South Alpine domain (N-Italy-Switzerland), *Contributions to Mineralogy and Petrology*, 96(2), 140-150,
 1987.
- 970 Stockar, R.: Facies, depositional environment, and palaeoecology of the Middle Triassic Cassina beds (Meride Limestone,
 Monte San Giorgio, Switzerland), *Swiss Journal of Geosciences*, 103(1), 101-119, [https://doi.org/10.1007/s00015-010-0008-](https://doi.org/10.1007/s00015-010-0008-2)
[2](https://doi.org/10.1007/s00015-010-0008-2), 2010.
- Stockar, R., Adatte, T., Baumgartner, P. O., and Föllmi, K. B.: Palaeoenvironmental significance of organic facies and stable
 975 isotope signatures: the Ladinian San Giorgio Dolomite and Meride Limestone of Monte San Giorgio (Switzerland, WHL
 UNESCO), *Sedimentology*, 60(1), 239-269, <https://doi.org/10.1111/sed.12021>, 2013.
- Storck, J. C., Brack, P., Wotzlav, J. F., and Ulmer, P.: Timing and evolution of Middle Triassic magmatism in the Southern
 Alps (northern Italy), *Journal of the Geological Society*, 176(2), 253-268, 2019.
- 980 Torsvik, T. H., and Cocks, L. R. M.: Earth geography from 400 to 250 Ma: a palaeomagnetic, faunal and facies review, *Journal*
of the Geological Society, 161(4), 555-572, 2004.
- Visonà, D.: Plutonismo basico ercinico nel Sudalpino delle Alpi Orientali: primi dati per un modello di tettonica a placche
 985 ercinica, *Rendiconti della Società geologica italiana*, 5(2), 105-107, <https://doi.org/10.1007/s005310100200>, 1982.
- Von Raumer, J., Stampfli, G., Borel, G., and Bussy, F.: Organization of pre-Variscan basement areas at the north-Gondwanan
 margin, *International Journal of Earth Sciences*, 91, 35-52, 2002.
- 990 Welch, B. L.: The generalization of 'Student's' problem when several different population variances are involved, *Biometrika*,
 34(1-2), 28-35, 1947.

- Willett, S. D., Herman, F., Fox, M., Stalder, N., Ehlers, T. A., Jiao, R., and Yang, R.: Bias and error in modelling thermochronometric data: resolving a potential increase in Plio-Pleistocene erosion rate, *Earth Surf. Dynam.*, 9, 1153-1221, <https://doi.org/10.5194/esurf-9-1153-2021>, 2021.
- Wilson, J.T.: Static or mobile Earth: The current scientific revolution, *Proceedings of the American Philosophical Society*, 112(5), 309–320, <https://www.jstor.org/stable/986051>, 1968.
- Wilson, R. W., Houseman, G. A., Buiter, S. J. H., McCaffrey, K. J., and Doré, A. G.: Fifty years of the Wilson Cycle concept in plate tectonics: an overview, *Geological Society, London, Special Publications*, 470(1), 1-17, <https://doi.org/10.1144/SP470-2019-58>, 2019.
- Winterer, E. L., and Bosellini, A.: Subsidence and sedimentation on Jurassic passive continental margin, Southern Alps, Italy, *AAPG bulletin*, 65(3), 394-421, <https://doi.org/10.1306/2F9197E2-16CE-11D7-8645000102C1865D>, 1981.
- Withjack, M. O., Islam, Q. T., and La Pointe, P. R.: Normal faults and their hanging-wall deformation: an experimental study, *AAPG bulletin*, 79(1), 1-17, 1995.
- Wolff, R., Dunkl, I., Kiesselbach, G., Wemmer, K., and Siegesmund, S.: Thermochronological constraints on the multiphase exhumation history of the Ivrea-Verbano Zone of the Southern Alps, *Tectonophysics*, 579, 104-117, <https://doi.org/doi:10.1016/j.tecto.2012.03.019>, 2012.
- Zanchetta, S., D'Adda, P., Zanchi, A., Barberini, V., and Villa, I. M.: Cretaceous-Eocene compression in the central Southern Alps (N Italy) inferred from 40Ar/39Ar dating of pseudotachylites along regional thrust faults, *Journal of Geodynamics*, 51(4), 245-263, <https://doi.org/doi:10.1016/j.jog.2010.09.004>, 2011.
- Zanchetta, S., Malusà, M. G., and Zanchi, A.: Precollisional development and Cenozoic evolution of the Southalpine retrobelt (European Alps), *Lithosphere*, 7(6), 662-681, <https://doi.org/doi:10.1130/L466.1>, 2015.
- Zanchi, A., Zanchetta, S., Berio, L., Berra, F., and Felletti, F.: Low-angle normal faults record Early Permian extensional tectonics in the Orobic Basin (Southern Alps, N Italy), *Italian Journal of Geosciences*, 138(2), 184-201, <https://doi.org/10.3301/IJG.2018.35>, 2019.

- 1025 Zanetti, A., Mazzucchelli, M., Sinigoi, S., Giovanardi, T., Peressini, G., and Fanning, M.: SHRIMP U–Pb zircon Triassic intrusion age of the Finero mafic complex (Ivrea–Verbano Zone, Western Alps) and its geodynamic implications, *Journal of Petrology*, 54(11), 2235–2265, 2013.
- Zanoni, D., and Spalla, M. I.: The Variscan evolution in the basement cobbles of the Permian Ponteranica Formation by microstructural and petrologic analysis, *Italian Journal of Geosciences*, 137(2), 254–271, <https://doi.org/10.3301/IJG.2018.12>, 2018.
- 1030 Zattin, M., Cuman, A., Fantoni, R., Martin, S., Scotti, P., and Stefani, C.: From Middle Jurassic heating to Neogene cooling: The thermochronological evolution of the southern Alps, *Tectonophysics*, 414(1–4), 191–202, <https://doi.org/10.1016/J.Tecto.2005.10.020>, 2006.
- 1035 Ziegler, P. A., and Stampfli, G. M.: Late Paleozoic–Early Mesozoic plate boundary reorganization: collapse of the Variscan orogen and opening of Neotethys, in: *Permian continental deposits of Europe and other areas. Regional reports and correlations*, edited by: Cassinis, G., Monografie di Natura Bresciana, Grafo, Brescia, Italy, 17–34, 2001.
- 1040 Zingg, A., Handy, M. R., Hunziker, J. C., and Schmid, S. M.: Tectonometamorphic history of the Ivrea Zone and its relationship to the crustal evolution of the Southern Alps, *Tectonophysics*, 182 (1–2), 169–192, [https://doi.org/10.1016/0040-1951\(90\)90349-D](https://doi.org/10.1016/0040-1951(90)90349-D), 1990.
- 1045 Zorn, H.: Paläontologische, stratigraphische und sedimentologische Untersuchungen des Salvatoredolomits (Mitteltrias) der Tessiner Kalkalpen: unter besonderer Berücksichtigung der Mikrofazies, Diagenese und Taxionomie der Lamellibranchiata, *Schweiz. Paläontol. Abh.*, 91, 1–90, 1971.
- Zwingmann, H., and Mancktelow, N.: Timing of Alpine fault gouges, *Earth and Planetary Science Letters*, 223(3–4), 415–425, <https://doi.org/10.1016/j.epsl.2004.04.041>, 2004.
- 1050